Differential Equation Models for Connected and Autonomous Vehicles

By

Shouwei Hui

DISSERTATION

Submitted in partial satisfaction of the requirements for the degree of

DOCTOR OF PHILOSOPHY

in

APPLIED MATHEMATICS

in the

OFFICE OF GRADUATE STUDIES

of the

UNIVERSITY OF CALIFORNIA

DAVIS

Approved:

Michael Zhang

Joseph Teran

Blake Temple

Committee in Charge

2024

To my parents, my friends, and myself

Contents

Abstract

This dissertation consists of three distinct but interconnected studies, each focusing on the modeling and stability analysis of Connected and Autonomous Vehicle (CAV) platoons under various traffic conditions. Using car-following (CF) models and macroscopic traffic flow models, this work explores how different platoon configurations, control strategies, and communication levels affect traffic flow stability in both homogeneous (fully autonomous) and mixed traffic environments.

The first study presents a novel approach to coordinated vehicle platooning, where the platoon followers communicate solely with the platoon leader. A dynamic model is proposed to account for driving safety under communication delays. General linear stability results are mathematically proven, and numerical simulations are performed to analyze the impact of model parameters in two scenarios: a ring road with initial disturbance and an infinite road with periodic disturbance. The simulation outcomes align with the theoretical analysis, demonstrating that the proposed "look-to-the-leader" platooning strategy significantly outperforms conventional car-following strategies, such as following one or two vehicles ahead, in terms of traffic flow stabilization. This study introduces a new perspective on organizing platoons for connected and autonomous vehicles, with implications for enhancing traffic stability.

In the second study, we extend the single platoon car-following (CF) model in chapter 2 to some multi-platoon CF models for connected and autonomous vehicles (CAVs) with flexible platoon sizes and communication levels. Specifically, we consider forward and backward communication methods between platoons with delays. Some general results of linear stability are mathematically proven, and numerical simulations are performed to illustrate the effects of platoon sizes and communication levels, as well as to demonstrate the potential for stabilizing human-driven vehicles (HDVs) in mixed traffic conditions. The simulation results are consistent with theoretical analysis, and demonstrate that in the ring road scenario, CAV platoons can stabilize certain percentage of HDVs. This study can provide suggestions for the design of communication system of autonomous vehicles (AVs), and management of mixed traffic flow of CAVs and HDVs.

In the final study, we extend the Aw-Rascle-Zhang (ARZ) non-equilibrium traffic flow model to take into account the look-ahead capability of connected and autonomous vehicles (CAVs), and the mixed flow dynamics of human driven and autonomous vehicles. The look-ahead effect of CAVs is captured by a non-local averaged density within a certain distance (the look-ahead distance). We

show, using wave perturbation analysis, that increased look-ahead distance loosens the stability criteria. Our numerical experiments, however, showed that a longer look-ahead distance does not necessarily lead to faster convergence to equilibrium states. We also examined the impact of spatial distributions and market penetrations of CAVs and showed that increased market penetration helps stabilizing mixed traffic while the spatial distribution of CAVs have less effect on stability. The results revealed the potential of using CAVs to stabilize traffic, and may provide qualitative insights on speed control in the mixed autonomy environment.

This dissertation provides theoretical insights and practical implications for the design of CAV control systems, with potential applications in stabilizing mixed traffic flows and improving vehicle coordination. The findings lay a foundation for future research on integrating advanced control strategies and extending the models to more complex traffic scenarios.

Acknowledgments

Firstly, I am profoundly grateful to my advisor, Professor Michael Zhang, for his invaluable insights, patience, and dedication, which have been instrumental in shaping my research and academic growth. Professor Zhang introduced me to the field of traffic flow research, providing guidance and support that has been essential throughout my six-year journey. I am immensely fortunate to have had the opportunity to work under his mentorship.

I would also like to extend my heartfelt thanks to my dissertation and qualification committee members: Professor Joseph Teran, Professor Blake Temple, Professor Qinglan Xia, and Professor Jia Li. Their expertise and insightful feedback have been crucial to the development of my research, and I deeply appreciate their efforts in evaluating and refining my work.

Next, I wish to acknowledge the generous support of the Department of Mathematics and the GGAM program. I am sincerely grateful to my initial advisor, Professor Robert Guy, and the other outstanding faculty members who have guided and inspired me throughout my Ph.D. journey. I am also deeply thankful to Tina Denera and the many other supportive staff members, whose kindness and assistance have made this journey smoother and more enjoyable.

It has been a great honor to share this journey with remarkable peers and friends at UC Davis. I am especially grateful to my friends in the Math and Statistics department, including Ye He, Jiaxiang Li, Chengyang Wang, Xiawei Wang, Tesi Xiao, Qianhui Wan, and many others, with whom I shared countless unforgettable moments over the past six years, particularly during the challenging pandemic period. I would also like to express my heartfelt appreciation to my labmates, including Hang Gao, Ashkan Teymouri, Yanlin Qi, Di Chen, Zenghao Hou, Shenyang Chen, Xianyue Peng, and many others, who have provided invaluable support and inspired me with research ideas. I am deeply honored to have had such wonderful people in my life throughout my Ph.D. journey.

The remote support from my close friends has also been an invaluable part of my academic experience. I am deeply grateful for the conversations, encouragement, and joyful moments shared with Wenbo Yu, Zhixin Guo, Kai Niu, Mengshen Liu, Xinyi Liu, Jiayi Chen and many others. Their companionship, even from afar, has been a source of strength.

Lastly, I extend my deepest gratitude to my parents, whose unwavering love, patience, and sacrifices have been the foundation of my achievements. They have been my constant source of

strength, always encouraging me to pursue my dreams and reminding me of the values of resilience, integrity, and compassion. Their support has not only been emotional but also a profound financial commitment, making it possible for me to follow this path without hesitation. This achievement is as much theirs as it is mine.

CHAPTER 1

A general introduction of traffic flow models

Traffic flow modeling has been a crucial topic in transportation research for nearly a century [16]. The goal of modeling traffic flow is to better understand and improve the movement of vehicles on road networks. As road congestion continues to grow and the demand for more efficient transportation systems rises, traffic flow models have become increasingly important for enhancing the safety, efficiency, and stability of traffic worldwide. Through traffic flow models, researchers and engineers can better analyse both individual and collective behavior of traffic dynamics, investigate causes of traffic congestion and evaluate different traffic control strategies. Broadly, traffic flow models are mainly classified into two categories: microscopic and macroscopic models.

1.1. Microscopic traffic flow models

Microscopic traffic flow models focus on individual vehicle behaviors and simulate the interaction between vehicles based on their microscopic properties, e.g. position, velocity and acceleration of each vehicle.

Car-following (CF) models are central to microscopic modeling, describing how a vehicle adjusts its speed in response to surrounding vehicles. They are often modeled by second-order ordinary differential equations (ODEs) where the acceleration variables are represented as functions of speed position variables.

Microscopic models are widely used for simulating platooning systems involving connected and autonomous vehicles (CAVs), where precise vehicle-to-vehicle interactions are critical. These models help in developing control strategies that improve traffic efficiency and safety by coordinating vehicle movements in both homogeneous and mixed traffic environments. However, they are computationally expensive in large-scale networks. More details will be provided in Chapter 2 and Chapter 3.

1.2. Macroscopic traffic flow models

Inspired by fluid dynamics [32], macroscopic traffic flow models take a broader approach by treating traffic as a continuous flow to focus on the collective behavior of vehicles. These models typically focus on aggregate variables such as traffic density, speed, and flow to capture large-scale patterns across traffic networks. They are often represented by hyperbolic partial differential equations (PDEs), which are derived from the principles of conservation laws and momentum [57].

Macroscopic models are particularly powerful for analyzing large-scale traffic management strategies, such as ramp metering and variable speed limits (VSL) [70, 71]. They can also be applied to mixed traffic environments involving both CAVs and human-driven vehicles (HDVs) [56]. While macroscopic models allow for efficient simulation of traffic over large networks, they lack the granularity needed to capture the behavior of individual vehicles. Further details on macroscopic models will be provided in Chapter 4.

1.3. Other models

Other than microscopic and macroscopic models, there are other type of traffic flow models including mesoscopic traffic flow model [8]. Mesoscopic models offers a middle ground of microscopic and macroscopic approaches by capturing some level of details in vehicle interactions without diving into details of every vehicle as in microscopic models. Multi-scale models, on the other hand, integrate microscopic and macroscopic elements to simulate detailed vehicle interactions in specific areas (e.g., slow vehicles as moving bottlenecks [9]) while maintaining a macroscopic perspective across the larger network. To account for uncertainties inherent in human driver behaviors and communication delays, stochastic models [22] and reinforcement learning (RL) based models [66] are increasingly explored to offer more insightful modelling and control strategies.

CHAPTER 2

ODE models: CF models for a single CAV platoon

2.1. Introduction

In recent years, Connected and Autonomous Vehicles (CAVs) have acquired significant global attention. With the fast development of CAV technologies and their supporting infrastructures, cooperative car-following (CF), including platooning, are poised to be implemented in the near future to enhance traffic flow. Platooning is a coordinated driving method for a group of vehicles that can be analysed as a systematic longitudinal traffic control system [58]. Such systems are typically modeled using microscopic traffic models, particularly those based on ordinary differential equations (ODEs).

Pipes [51] was among the first to introduce car-following models in 1953, which described the behavior of a string of cars. Since then, numerous car-following models with adjustable parameters have been developed. Bando et al. [2,3] proposed the Optimal Velocity Model (OVM) that replaces the velocity of the lead vehicle in Pipes' model with an optimal velocity function. In particular, OVM can capture traffic instabilities on a ring road without external disturbances. Treiber et al. [62] introduced the Intelligent Driver Model (IDM), which further accounts for the velocity difference of the lead vehicle. These models are widely used in traffic simulations and control design since they are able to represent typical traffic phenomena in relatively simple forms.

The aforementioned models only describe the interaction between two vehicles in a leader-follower configuration. Several extensions have been developed based on these models. Lenz et al. [31] introduced a multi-following model based on OVM, which considers the influence of multiple vehicles ahead. Nakayama et al. [43] proposed a backward-looking model, also based on OVM, to capture the effect of the vehicle behind on the subject vehicle. Jiang et al. [24] introduced the Full Velocity Difference Model (FVDM), which accounts for both positive and negative relative velocity to eliminate unrealistic acceleration and deceleration behaviors. Yu et al. [72] extended FVDM by incorporating acceleration differences. Lazar et al. [27] provided a comprehensive review

of OVM-based models from 1995 to 2016. Treiber et al. [63] expanded the IDM to follow multiple vehicles ahead while considering reaction time and estimation errors. Derbel et al. [10] proposed a modified version of IDM that enhances vehicle performance and safety.

Car-following models can be integrated with various control designs to evaluate the impact of CAVs within a mixed traffic environment consisting of both human-driven and autonomous vehicles. Zhu and Zhang [85] modified OVM by introducing a smoothing factor to model autonomous vehicles (AVs) and analyzed mixed traffic involving both AVs and human-driven vehicles (HDVs). Jia and Ngoduy [23] developed a platoon-controlled car-following model based on realistic inter-vehicle communication and designed a consensus-based control system for multiple platoons moving in unison. Zhang et al. [77] extended Zhu's model for platooned CAVs by combining multi-following with weighted relative velocity differences and analyzed the linear stability of the model. Wang et al. [67] proposed Leading Cruise Control (LCC), a mixed traffic flow control strategy for CAVs that allows them to adaptively follow the vehicle ahead while pacing the following vehicles. Zhao et al. [78] introduced safety-critical traffic control (STC), where CAVs maintain safety relative to both the preceding vehicle and following HDVs, with HDVs modeled using OVM in both Wang's and Zhao's papers. Zhou et al. [83,84] proposed a platoon-based Intelligent Driver Model (P-IDM) along with an Autonomous Platoon Formation Strategy (APFS) to stabilize CAV platoons under periodic disturbances. Jin and Meng [25] presented a model combining OVM with a time-delayed feedback controller, increasing stability by analyzing the transcendental characteristic equation to eliminate unstable eigenvalues. Sun et al. [61] examined the relationship between string instability in IDM-based controllers and traffic oscillations, identifying optimal parameters for CAVs to improve stability by forming finite-sized platoons.

Theoretically, beyond car-following models, methodologies such as stochastic modeling, constrained optimization, and model predictive control (MPC) have also been applied by traffic researchers to address CAV platooning problems. Li [33, 34] proposed a stochastic dynamic model for vehicle platoons and investigated its statistical characteristics. Gong et al. [14] introduced a multi-agent dynamic system to model platoons, with the control scheme formulated as a constrained optimization problem. Zhou et al. [82] developed a series of distributed MPC strategies for coordinated car-following of CAVs, providing approaches that ensure local, L_2, and L_∞ stabilities. Graffione et al. [15] introduced an MPC approach to control inter-vehicular distances and

speed within a vehicle platoon, which improves safety and reduces fuel consumption. Li et al. [35] developed a platoon control strategy for heterogeneous connected vehicles (CVs) by incorporating a variable time headway (VTH) spacing policy and a sliding mode controller. Liu et al. [37] adopted an integrated deep reinforcement learning (DRL) and dynamic programming (DP) approach to learn autonomous platoon control policies.

Field experiments and related data analysis can further demonstrate the effectiveness of CAVs and CAV platoons in stabilizing traffic and reducing fuel consumption. Stern et al. [59] conducted a ring road experiment with over 20 vehicles, showing that a controlled autonomous vehicle can dampen stop-and-go waves, reducing total fuel consumption. Lee et al. [30] implemented a large-scale field experiment involving 100 CAVs functioning as a MegaController on a freeway network to mitigate stop-and-go waves, marking the largest CAV field experiment to date. Tsugawa et al. [64] tested a platoon of three trucks on a test track along an expressway, demonstrating a 14% reduction in fuel consumption. By combining experimental datasets, Zhou et al. [81] investigated the emissions and fuel consumption (EFC) characteristics in car-following (CF) platoons.

In general, previous studies on CAV platoon control have demonstrated the potential of CAVs in stabilizing traffic, particularly by developing car-following models that enhance traffic stability through advanced control and communication strategies. However, most existing models rely on communication with multiple vehicles, which increases system complexity and communication load, especially in mixed-traffic conditions. Additionally, few studies prioritize a platoon structure that optimally reduces inter-vehicle communication requirements while maintaining robust stability. Motivated by these research gaps,, in this chapter we make several contributions to CAV platoon control. We propose a novel platoon CF model that enhances traffic stability by focusing on coordinated communication strategies, particularly prioritizing the role of the leading vehicle. We also show the superiority of our models by performing rigorous mathematical stability proofs and comprehensive numerical simulations. The simulations cover a variety of traffic scenarios, demonstrating how different parameters can impact the stability of a single platoon. Our findings indicate that the proposed control strategy significantly outperforms conventional methods in suppressing traffic oscillations and maintaining string stability.

The remaining parts of this chapter are organized as follows. In section 2.2, the car-following models for HDVs and platoon-controlled CAVs are introduced. In section 2.3, linear stability

criteria of the proposed models are presented and proved. In section2.4, numerical simulations on a ring road and an infinite road are demonstrated and performances of different model parameters are evaluated. Lastly in section 2.5, the conclusion is drawn and potential directions for future research are discussed.

2.2. The Non-Platoon and Platoon CF Models

Without loss of generality, we assume a string of N vehicles are moving along a single-lane road without overtaking. The initial position of the rear bumper of the first vehicle is at 0m of the road, with the leading vehicle designated as N-th vehicle. In particular, if the single-lane road is a ring road, the $(N+1)$-th vehicle is the same as the 1st vehicle. To demonstrate the effectiveness of the platoon-controller for connected and autonomous vehicles (CAV), we introduce a base model for human-driven vehicles (HDVs) in Section 2.2.1. In Section 2.2.2, we present the model for platoon-controlled CAVs, followed by a transition phase model in Section 2.2.3.

2.2.1. Optimal velocity model . A commonly used car-following model to represent human-driven vehicles (HDVs) is the Optimal Velocity Model (OVM) [3]. OVM has the form

$$\ddot{x}_i(t) = a\left[V(x_{i+1}(t) - x_i(t)) - \dot{x}_i(t)\right], \tag{2.1}$$

where $x_i(t)$, $i = 1, 2, \ldots N$ is the position of i-th vehicle at time t on the single-lane road without overtaking. $x_{i+1}(t) - x_i(t) \triangleq h_i(t)$ is the headway between the i-th and $i+1$-th vehicle. $\dot{x}_i(t)$, $\ddot{x}_i(t)$ are velocity and acceleration of i-th vehicle at time t, $V(h)$ is the optimal velocity function of headway (head to head distance) h, and a is a sensitivity constant. An example of optimal velocity function is given in [67], which is equivalent to the form

$$V(h) = \begin{cases} v_{\max}, & \text{if } h \geq h_{\max}; \\ \frac{v_{\max}}{2}\left(1 - \cos\left(\pi \frac{h - h_{\min}}{h_{\max} - h_{\min}}\right)\right), & \text{if } h_{\min} \leq h \leq h_{\max}; \\ 0, & \text{if } h \leq h_{\min}, \end{cases} \tag{2.2}$$

where $h_{\min}$ is the minimum headway, $h_{\max}$ is the maximum headway, $v_{\max}$ is the maximum velocity and l is the length of each vehicle. Figure 2.1 is an example plot of 2.2 and the corresponding fundamental diagram (density-flow diagram).

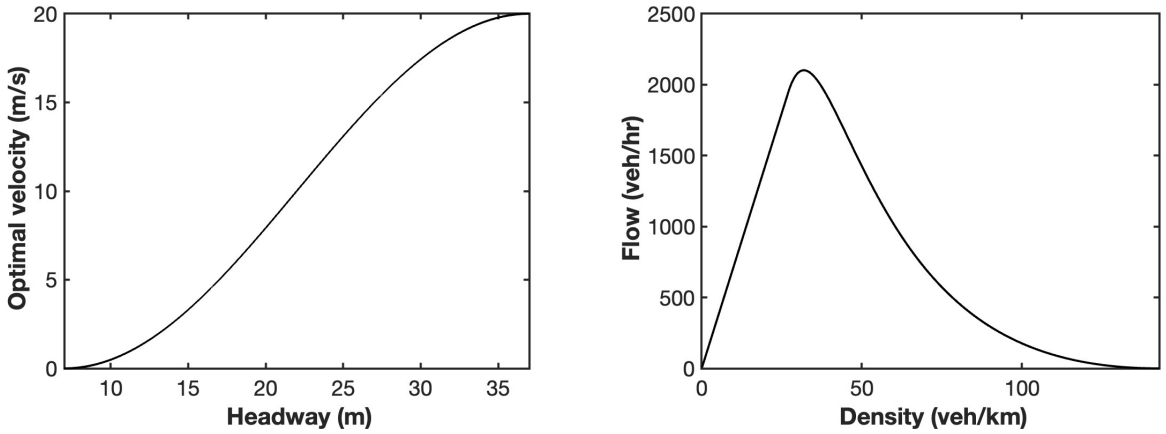

(a) Optimal velocity function (b) Fundamental diagram

FIGURE 2.1. Plot of an optimal velocity function with $l = 5\text{m}$ and $v_{\max} = 20\text{m/s}$ and the corresponding fundamental diagram.

2.2.2. Platoon controller: A coordinated car-following strategy . We now consider a system of CAVs where every following vehicle is connected to the leading autonomous vehicle. In this setup, the following vehicles have access to the position and speed of the leading vehicle. In the proposed platoon model, only the position information of the leading vehicle is required. We further assume that the target (optimal) velocity of a following vehicle in the platoon is based on its distance from the leading vehicle:

$$\ddot{x}_i(t) = a\left[V(\frac{x_N(t) - x_i(t)}{N - i}) - \dot{x}_i(t)\right], \tag{2.3}$$

where x_N is the position of the controlled leading vehicle. We refer 2.3 as the platoon controlled OVM (P-OVM) model. In this model, the spacing between the platoon leader (the N-th vehicle) and the i-th following vehicle is scaled and used in the optimal velocity function. This is equivalent to considering the average spacing of vehicles between the platoon leader and the i-th following vehicle. Figure 2.2 illustrates this platoon-controlled car-following configuration. Notably, under this setup, the influence of the immediate preceding vehicle is neglected, which could potentially result in collisions if position measurement errors or communication delays between the platoon leader and the following vehicles reach a critical threshold.

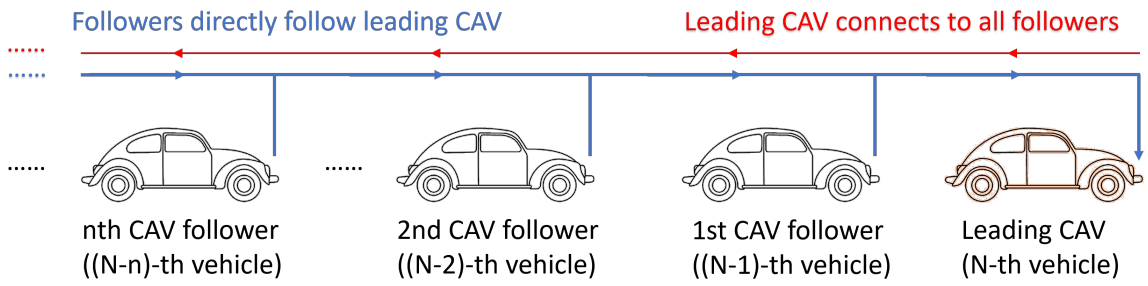

FIGURE 2.2. Illustration of the platoon-controlled car-following system. Leading CAV is connected to all followers of the platoon and followers are directly following the leading CAV

2.2.3. The transition phase model . We can address the previously mentioned safety issue by adding a local, within platoon vehicle-to-vehicle control to P-OVM. This local control can be any feedback mechanism that prevents vehicle collisions. For the sake of simplicity in presentation and analysis, we adopt OVM as the local control mechanism, referring to the combined model as the Transition Phase Optimal Velocity Model (T-OVM). The model is of the form

$$\ddot{x}_i = a(V(x_{i+1} - x_i) - \dot{x}_i) + b\left(V\left(\frac{x_N - x_i}{N - i}\right) - \dot{x}_i\right), \tag{2.4}$$

where a is the sensitivity to vehicle in front and b is the sensitivity to the leading vehicle. The total sensitivity is defined as the sum of the sensitivities $(a + b)$. Figure 2.3 illustrates the car-following pattern of the T-OVM. With this two-part model, each vehicle within the platoon balances between maintaining the optimal velocity relative to the vehicle directly in front and the optimal velocity relative to the platoon leader. This balance helps prevent collisions while simultaneously enhancing stability.

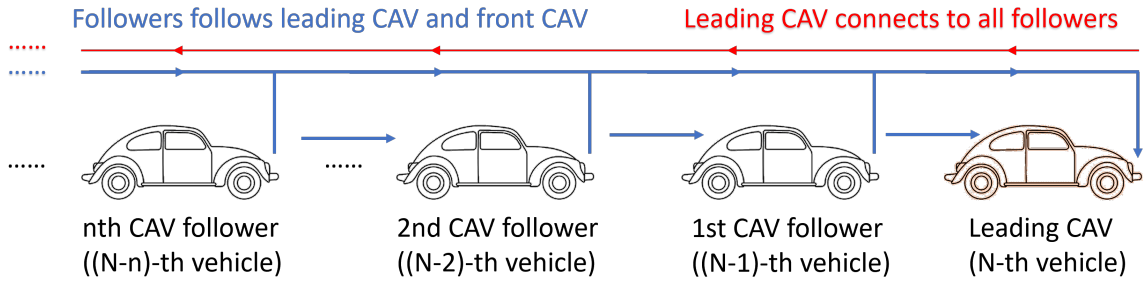

FIGURE 2.3. Illustration of the transition phase car-following system. Leading CAV is connected to all followers inside the platoon and followers are following the leading CAV and the front CAV simultaneously

2.3. Stability analysis of the platoon models

If the string of N vehicles are on a ring road with length L and the leading vehicle is following the last vehicle of the string by the original OVM 2.1, the position of $i-th$ vehicle is the same for both OVM 2.1 and P-OVM 2.5 under steady state:

$$e_i(t) = hi + V(h)t, \tag{2.5}$$

where $h = L/N$ is the equilibrium headway. For the classic optimal velocity model, we have the following linear stability criterion:

THEOREM 2.3.1. *The optimal velocity model 2.1 is linearly stable if*

$$a > 2V'(h). \tag{2.6}$$

A proof slightly different from [3] is given in Appendix A.1. Then with the platoon controller applied, it turns out that no stability criteria is required:

THEOREM 2.3.2. *In the N-vehicle platoon where the leader vehicle follows the last vehicle of the platoon on a ring road according to OVM (2.1), the platoon-controlled system P-OVM (2.3) is always linearly stable.*

PROOF. From previous introduction, P-OVM has the same equilibrium solution of the optimal velocity model as $x_n^0(t) = e_n(t)$ for any car n inside the platoon. Now suppose that all the vehicles are deviated from the initial position with a small disturbance $y_n(t)$, that is,

$$x_n(t) = e_n(t) + y_n(t),\ |y_n| \ll 1. \tag{2.7}$$

To linearize the original system, we can do a Taylor expansion of the optimal velocity function term $V(\Delta x_n)$ and neglect the higher order terms to get

$$\ddot{y}_n(t) = \begin{cases} a\left[V'(h)\frac{y_N(t)-y_n(t)}{N-n} - \dot{y}_n(t)\right], \text{ if } n \neq N; \\ a\left[V'(h)(y_1(t) - y_N(t)) - \dot{y}_N(t)\right], \text{ if } n = N. \end{cases} \tag{2.8}$$

Then by the formation of the controller, y_1 and y_N forms a system of 2 linear ODEs, and the solution in vector form is:

$$\mathbf{Y} = \sum_{n=1,\ N} C_n e^{\lambda_n t} \mathbf{V}_n, \tag{2.9}$$

where $Y = [y_1, y_N]^T$ is the vector form, λ_n and V_n are the eigenvalues and eigenvectors of the system, and C_n are constants determined by the initial condition. Now suppose that λ is an eigenvalue of the system, and ξ_n is the coefficient of y_n with the term $e^{\lambda t}$, then simplified from (2.8), λ satisfies

$$\lambda^2 + a\lambda - aV'(h)(\frac{\xi_1}{\xi_N} - 1) = 0, \tag{2.10}$$

and

$$\lambda^2 + a\lambda - aV'(h)(\frac{\xi_N}{(N-1)\xi_1} - \frac{1}{N-1}) = 0. \tag{2.11}$$

Then by comparing these equations we can calculate that $\xi_1 = \xi_N$ or $\xi_1 = -\xi_N/(N-1)$. And the first case is only true if we have $y_1 = y_N$ and the two cars just stay at the same distance from the original equilibrium. For the other case we have

$$\lambda^2 + a\lambda - aV'(h)(-\frac{1}{N-1} - 1) = 0. \tag{2.12}$$

Then, by solving the quadratic equation, we have

$$\lambda = \frac{-a \pm \sqrt{a^2 + 4aV'(h)(-\frac{1}{N-1} - 1))}}{2}. \tag{2.13}$$

For the system to be stable, we need to have the real parts of both λ to be negative. This is true if $V'(h) > 0$ which is always true for any well-defined $V(h)$. Now we just need to check if the same property holds for the remaining vehicles. By (2.8) we can have a initial guess that the nonlinear part is $y_j = \zeta y_N$ for $j \neq 1$, then plug this into (2.8) and compare the coefficients we have

$$\zeta = N - j + \frac{j-1}{N-1}. \tag{2.14}$$

Thus the other cars also have the same eigenvalue for the nonlinear part and the system will always be linearly stable if the problem is well defined. □

As for the transition phase model, stability clearly depends on both a, b and N. For N sufficiently large we have the following stability criterion:

THEOREM 2.3.3. *Assuming that the leading vehicle follows the last vehicle by OVM (2.1) with sensitivity constant $a+b$. Then the transition phase model T-OVM (2.4) is linearly stable if*

$$\frac{(a+b)^2}{a} > 2V'(h). \tag{2.15}$$

The proof is given in Appendix A.2. Figure 2.4 shows the plot of neutral stability lines for different sensitivity values. The area above the lines represents stability, while the area below indicates instability. From the figure, it is evident that as the value of b increases, the unstable area becomes smaller and eventually disappears when $a \to 0$.

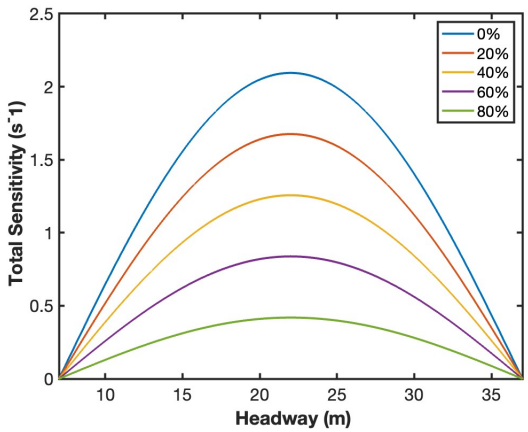

FIGURE 2.4. neutral stability lines of the transition phase model for selected percentages of leading vehicle sensitivity $b/(a+b) = 0\%, 20\%, 40\%, 60\%, 80\%$. Above each line the region is stable and below is unstable.

2.4. Numerical simulations

To better visualize how stability improves with the application of platoon control, several numerical experiments are conducted using different road configurations and model parameters. All simulations are performed in MATLAB 2023b, with a time step of $\Delta t = 0.1$s. The forward Euler scheme is used to update the velocity variable $\dot{x}_i$ and a modified Euler scheme (Heun's

method) is employed to update the position variable x_i:

$$\begin{cases} \dot{x}_{i,j+1} = \dot{x}_{i,j} + \ddot{x}_{i,j}\Delta t; \\ x_{i,j+1} = x_{i,j} + \frac{\dot{x}_{i,j}+\dot{x}_{i,j+1}}{2}\Delta t, \end{cases} \tag{2.16}$$

where $x_{i,j}$ is referring to the position of i-th car at j-th time step of simulation. This is equivalent to the discretizaiton method in [85].

2.4.1. Ring road with initial disturbance. In this subsection, simulations are conducted on a ring road with a total length of the ring road is $L = 264$m with 12 vehicles. For model parameters, we use the optimal velocity function given by (2.2) setting $h_{\min} = 7$m, $h_{\max} = 37$m, $v_{\max} = 20$m/s and $l = 5$m. This results in an equilibrium headway $h = L/N = 22$m and an equilibrium velocity $V(h) = 10$ m/s. The initial position and velocity of the i-th vehicle deviate from the equilibrium states $(e_i, V(h))$ with random perturbation uniformly distributed on the interval $[0, 5]$. The initial condition of the model can be written as

$$\begin{cases} x_i(0) = & e_i(0) + r_i; \\ \dot{x}_i(0) = & V(h) + \overline{r}_i, \end{cases} \tag{2.17}$$

where $r_i, \overline{r}_i$ are random numbers generated from uniform distribution on $[0, 5]$, and $e_i(0) = hi$ can be calculated from 2.5.

Simulation 1.1: Comparison between OVM and P-OVM

To demonstrate the stability improvement of P-OVM, we tested sensitivity constants $a =$ 0.4, 0.8, 1.6, 2.4 for both OVM and P-OVM under the same initial conditions. Simulation results are shown for the original OVM and platoon-controlled OVM in Figures 2.5-2.8. Figures 2.5, 2.6 are the 3-D plots of headways of all vehicles under OVM and P-OVM, respectively, with different values of a. Figures 2.7, 2.8 are the velocity profiles of the 6th vehicle under OVM and P-OVM, respectively, with different values of a.

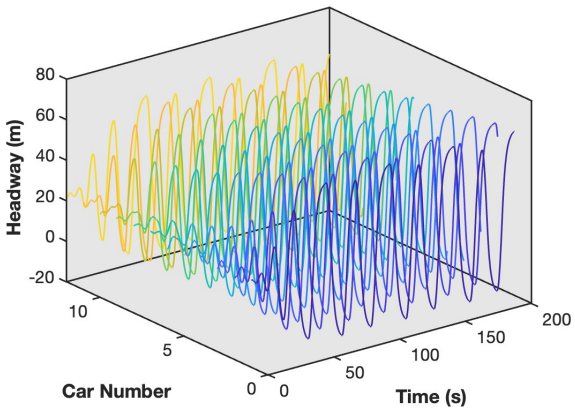

(a) $a = 0.4$

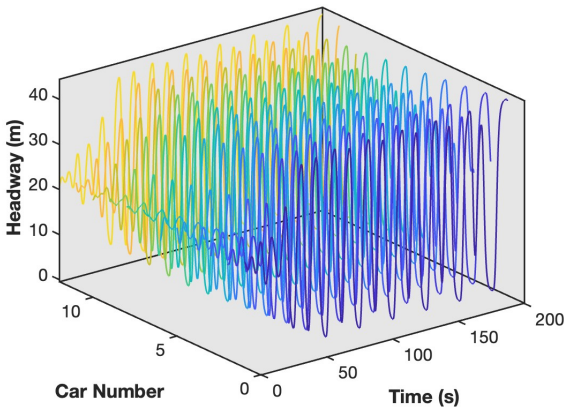

(b) $a = 0.8$

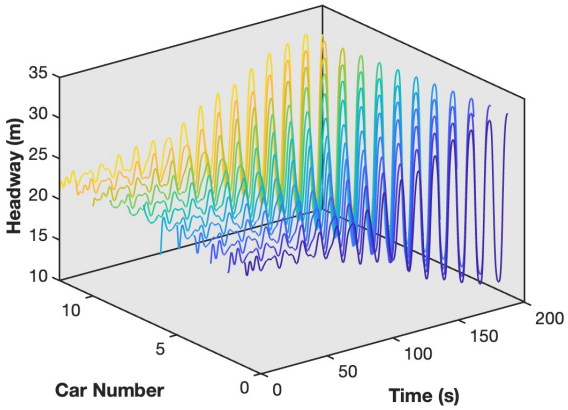

(c) $a = 1.6$

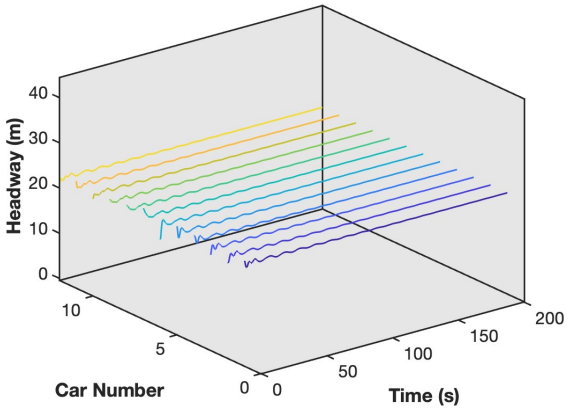

(d) $a = 2.4$

FIGURE 2.5. Headway profile of OVM with sensitivity constant $a = 0.4,\ 0.8\ , 1.6,\ 2.4$

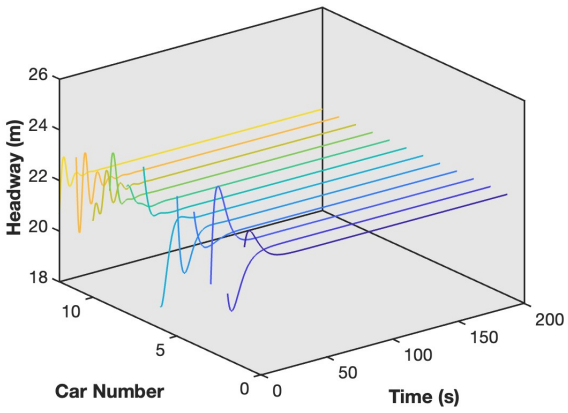

(a) $a = 0.4$

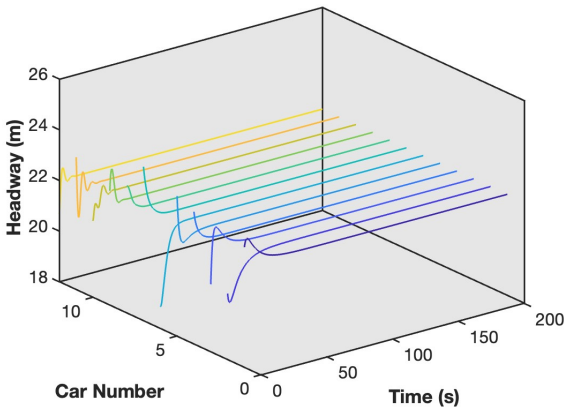

(b) $a = 0.8$

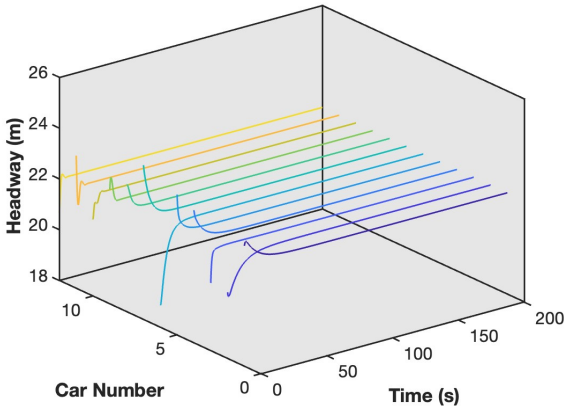

(c) $a = 1.6$

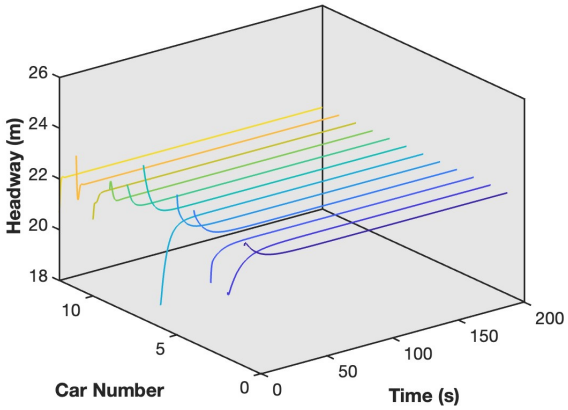

(d) $a = 2.4$

FIGURE 2.6. Headway profile of P-OVM with sensitivity constant $a = 0.4,\ 0.8\ , 1.6,\ 2.4$

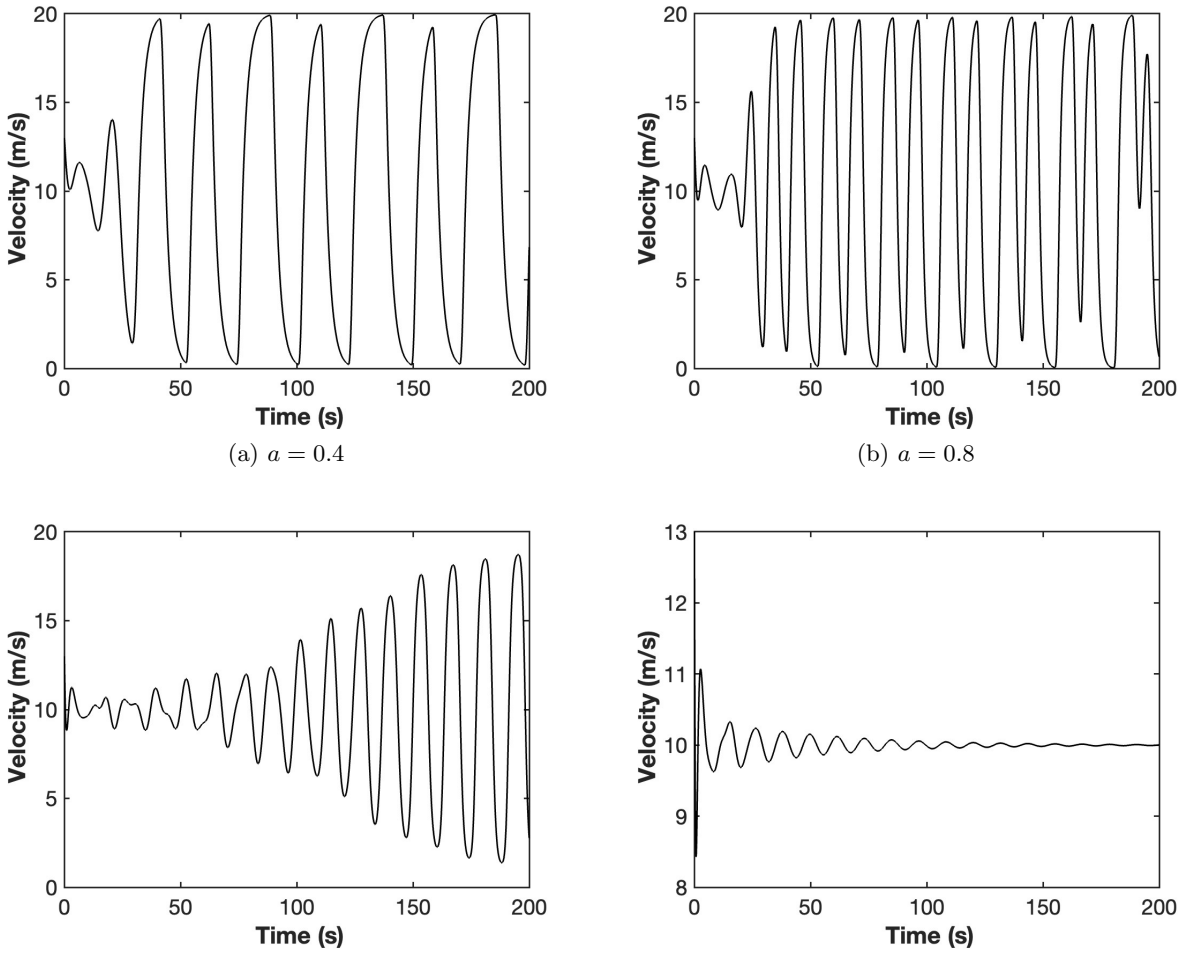

(a) $a = 0.4$

(b) $a = 0.8$

(c) $a = 1.6$

(d) $a = 2.4$

FIGURE 2.7. Velocity profile of 6th vehicle of OVM with sensitivity constant $a = 0.4,\ 0.8\ , 1.6,\ 2.4$

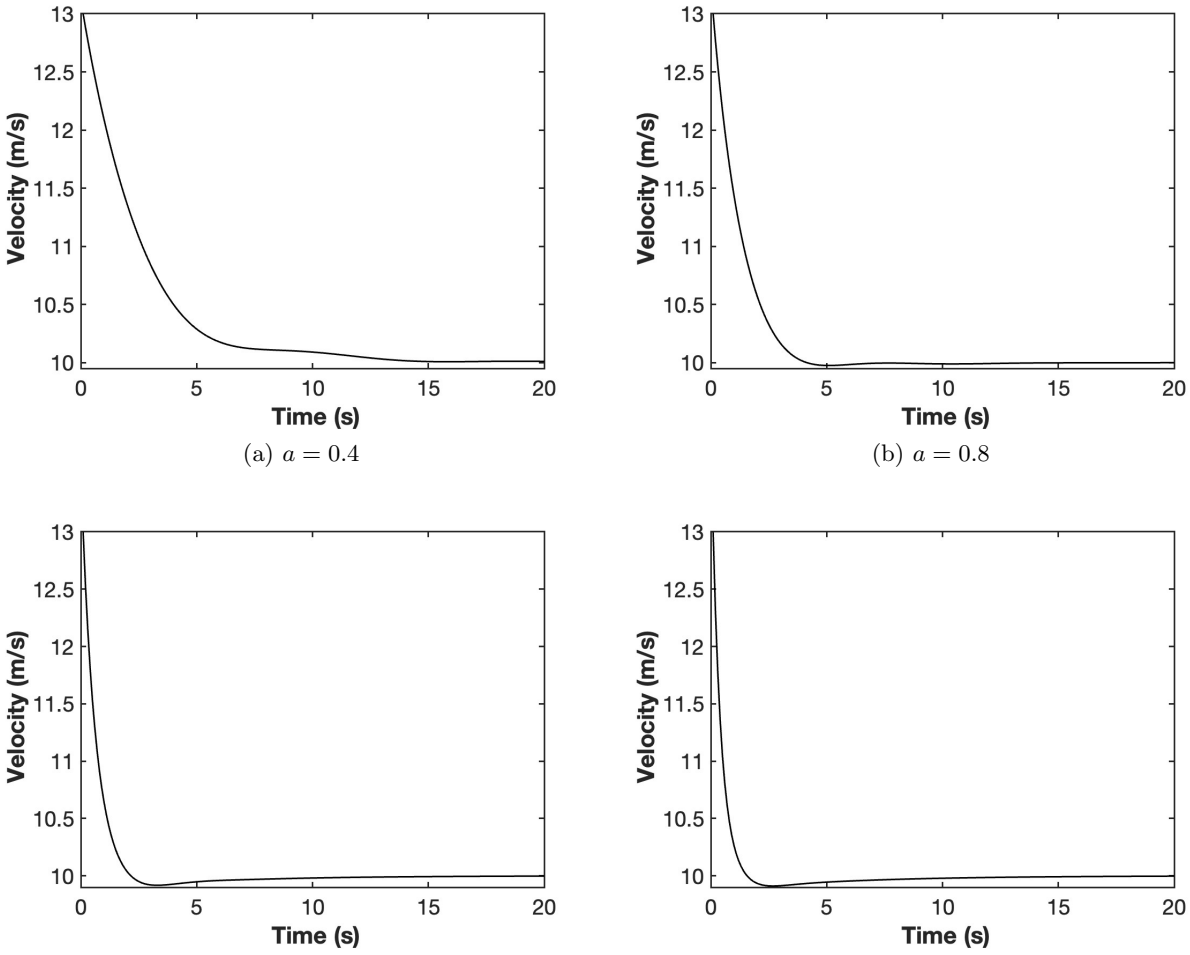

(a) $a = 0.4$ (b) $a = 0.8$

(c) $a = 1.6$ (d) $a = 2.4$

FIGURE 2.8. Velocity profile of 6th vehicle of P-OVM with sensitivity constant $a = 0.4,\ 0.8\ , 1.6,\ 2.4$

The simulation results show that the OVM is unstable for $a = 0.4,\ 0.8,\ 1.6$. At $a = 0.4$, negative headway are generated, indicating a risk of collisions due to low sensitivity. For $a = 2.4$ although the OVM is stable, the initial acceleration for the selected vehicle is unrealistically high. In contrast, the P-OVM remains stable for all selected values of a the model is stable and a with sensitivity primarily affecting the convergence speed. For greater values of a, traffic converge to the equilibrium state faster. Yet when a is sufficiently large, further improvements in convergence become negligible, as the original OVM is already stable.

Simulation 1.2: Test of T-OVM parameters

To test the performance of T-OVM, four cases of sensitivity pair: $(a, b) = (0.5, 0.1)$, $(0.1, 0.5)$, $(1, 0.2)$, $(0.6, 0.6)$ are tested under the same initial conditions. The extreme cases where $a = 0$ or $b = 0$ are not considered as they essentially reduce to OVM or P-OVM, respectively. Simulation results are in Figures 2.9-2.10. Figure 2.9 is the headway profile of all 12 vehicles in 3-D plot with different pairs of sensitivity constants, and Figure 2.10 is the velocity profile of the 6th vehicle.

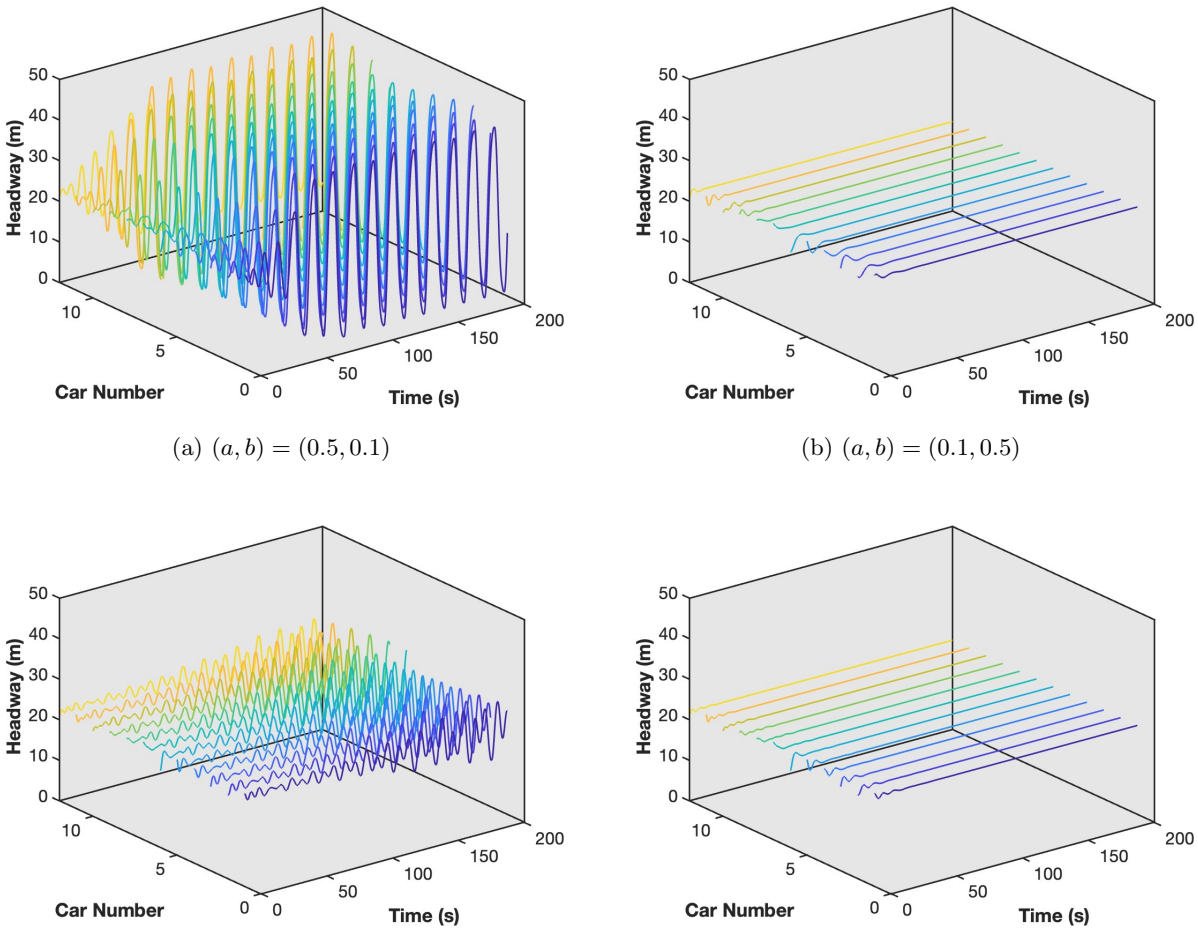

(a) $(a, b) = (0.5, 0.1)$

(b) $(a, b) = (0.1, 0.5)$

(c) $(a, b) = (1, 0.2)$

(d) $(a, b) = (0.6, 0.6)$

FIGURE 2.9. Headway profile of T-OVM with sensitivity constant $(a, b) = (0.5, 0.1), (0.1, 0.5), (1, 0.2), (0.6, 0.6)$

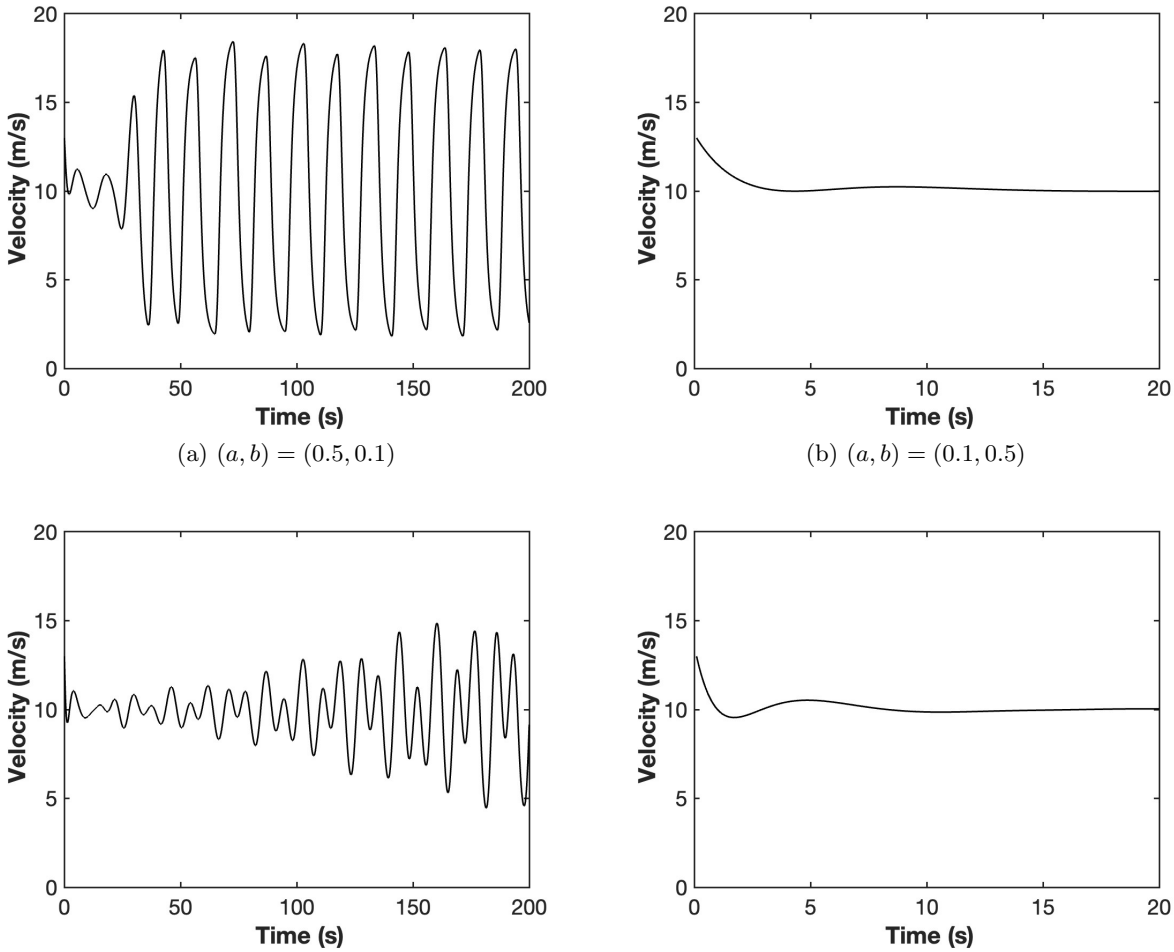

(a) $(a, b) = (0.5, 0.1)$ (b) $(a, b) = (0.1, 0.5)$

(c) $(a, b) = (1, 0.2)$ (d) $(a, b) = (0.6, 0.6)$

FIGURE 2.10. Velocity profile of 6th vehicle of T-OVM with sensitivity constant $(a, b) = (0.5, 0.1), (0.1, 0.5), (1, 0.2), (0.6, 0.6)$

The simulation results show that as the percentage of sensitivity to the leading vehicle increases, the traffic stream becomes more stable. Additionally, for higher total sensitivity $(a + b)$ lower percentages of leading vehicle sensitivity is required to achieve string stability, which aligns with the theoretical results (see figure 2.4).

Simulation 1.3: Comparison of T-OVM with two cars ahead following

To show the effectiveness of following the platoon leader, we compare the T-OVM 2.4 with the front multi-following OVM (F-OVM) of two cars in [31]:

$$\ddot{x}_i = a(V(x_{i+1} - x_i) - \dot{x}_i) + b\left(V\left(\frac{x_{i+2} - x_i}{2}\right) - \dot{x}_i\right), \tag{2.18}$$

where the sensitivity b is for the second vehicle in front. Two cases of sensitivity pair: $(a, b) = (0.8, 0.4), (0.2, 0.4)$ are tested. Simulation results are in Figures 2.11, 2.12. Figure 2.11 is the headway profile of all 12 vehicles in 3-D plot with T-OVM and F-OVM and Figure 2.12 is the velocity profile of the 6th vehicle.

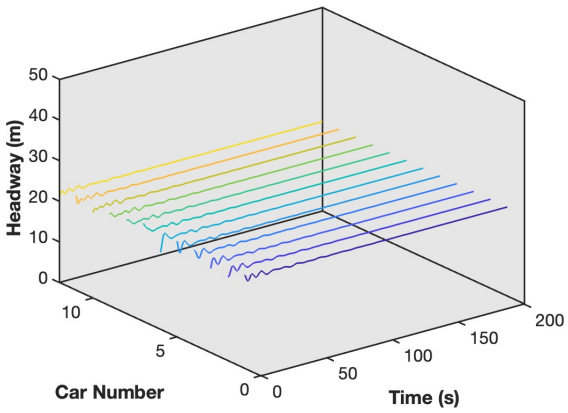

(a) T-OVM with $(a, b) = (0.8, 0.4)$

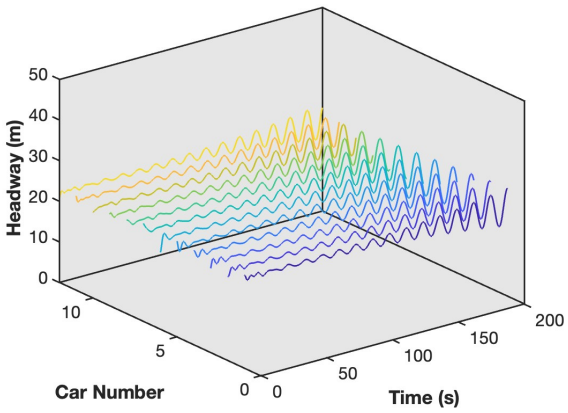

(b) F-OVM with $(a, b) = (0.8, 0.4)$

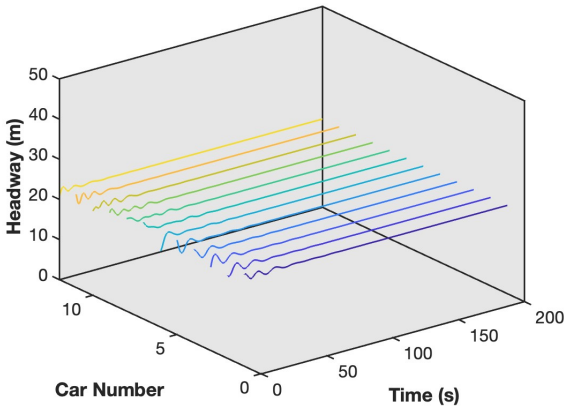

(c) T-OVM with $(a, b) = (0.2, 0.4)$

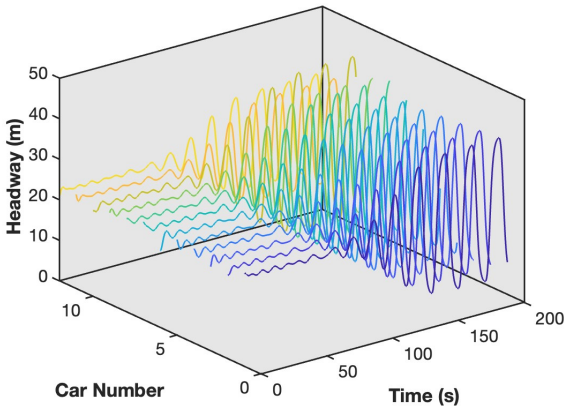

(d) F-OVM with $(a, b) = (0.2, 0.4)$

FIGURE 2.11. Headway profile of T-OVM and F-OVM with sensitivity constant $(a, b) = (0.8, 0.4), (0.2, 0.4)$

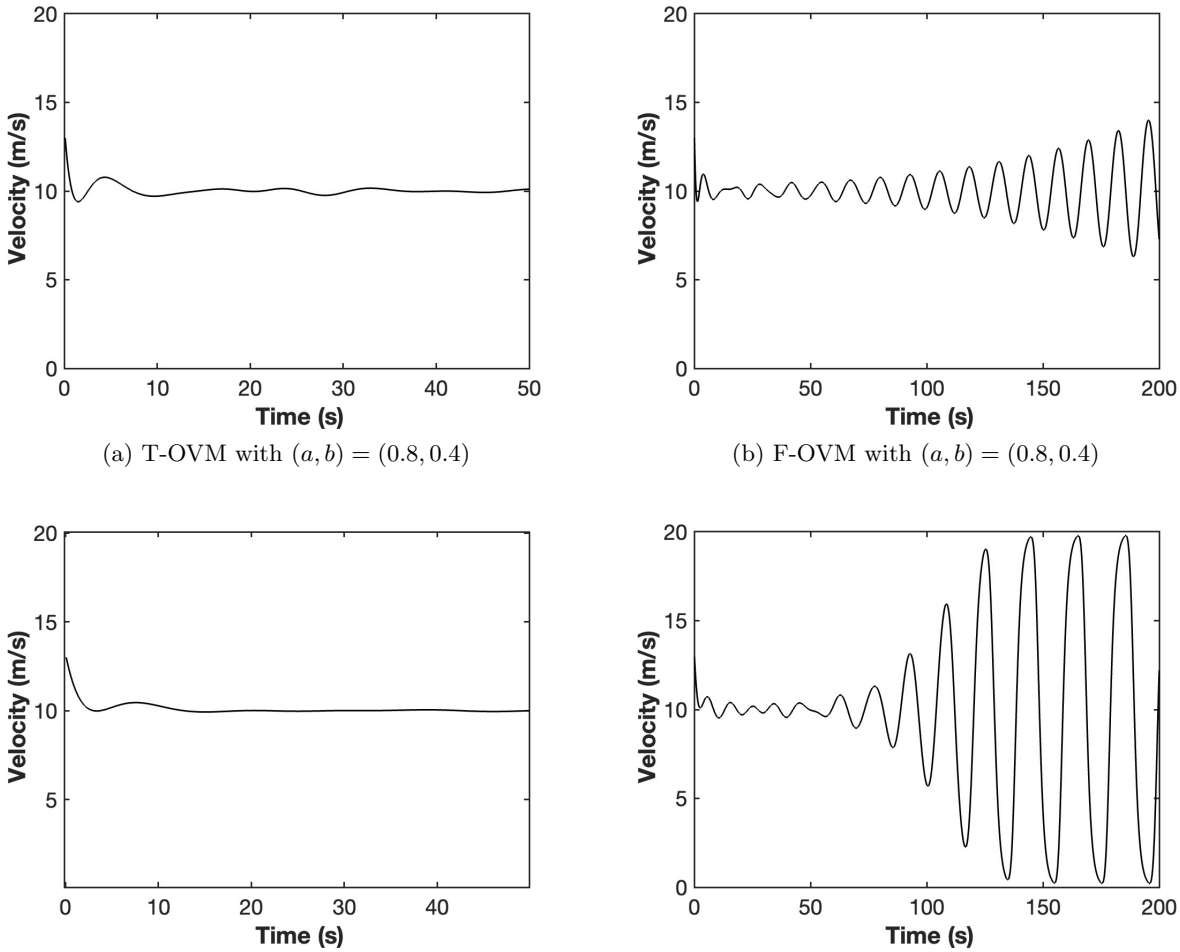

(a) T-OVM with $(a, b) = (0.8, 0.4)$

(b) F-OVM with $(a, b) = (0.8, 0.4)$

(c) T-OVM with $(a, b) = (0.2, 0.4)$

(d) F-OVM with $(a, b) = (0.2, 0.4)$

FIGURE 2.12. Velocity profile of 6th vehicle of T-OVM and F-OVM with sensitivity constant $(a, b) = (0.8, 0.4), (0.2, 0.4)$

From the simulation results we can observe that for the same setting of sensitivity parameters, T-OVM can suppress the disturbance and the platoon remains stable while F-OVM cannot. Furthermore, the stabilizing effect of the T-OVM becomes more prominent when the following vehicles respond more strongly to the leader in the T-OVM, while the destabilizing effect in the F-OVM becomes stronger when the following vehicle respond more strongly to the second vehicle ahead. These findings demonstrate the superiority of applying T-OVM in stabilizing CAV platoons.

2.4.2. Infinite road with periodic disturbance. In addition to the initial disturbance, it is also valuable to examine whether platoon control can enhance stability under periodic disturbances. In this subsection we consider $N = 10$ vehicles travelling on an infinite road with a free flow speed

of $v_{max} = 30\text{m/s}$ and a uniform length of $l = 5\text{m}$. The optimal velocity function $V_I(h)$ for the infinite road simulation is equivalent to a triangular fundamental diagram:

$$V_I(h) = \begin{cases} v_{\max}, & \text{if } \rho(h) \leq \rho_c; \\ \frac{v_{\max} * \rho_c(\rho(h) - \rho_{\max})}{\rho(h)(\rho_c - \rho_{\max})}, & \text{if } \rho_c \leq \rho(h) \leq \rho_{\max}; \\ 0, & \text{if } \rho \geq \rho_{\max}, \end{cases} \tag{2.19}$$

where $\rho(h) = l/h$ is the occupancy of vehicles on the road where $\rho = 0$ indicates an empty road, and $\rho = 1$ represents full vehicle occupancy. $\rho_c = 5/37$ is the critical occupancy where flow is maximized and $\rho_{\max} = 5/7$ is the jam occupancy. Figure 2.13 is a plot of the optimal velocity function and corresponding triangular fundamental diagram.

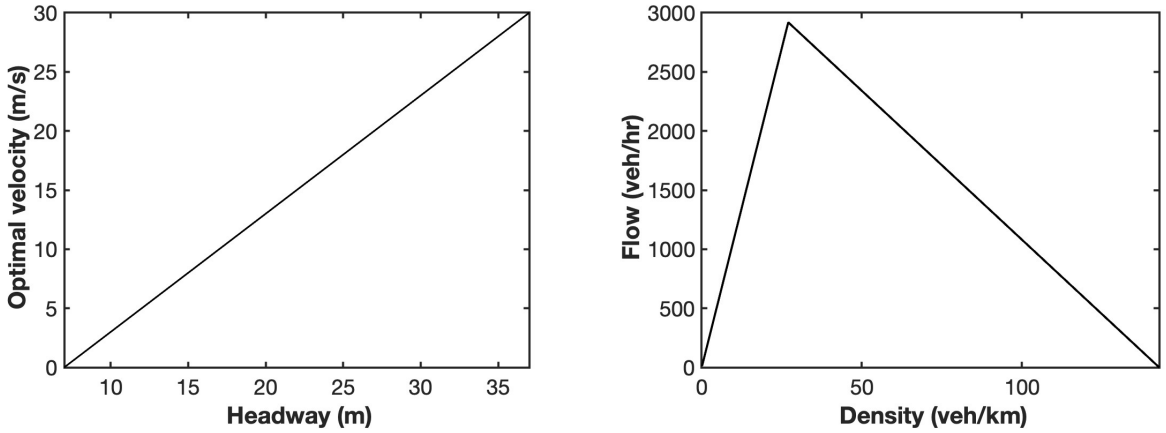

(a) Optimal velocity function

(b) Triangular fundamental diagram

FIGURE 2.13. Plot of an optimal velocity function with $l = 5\text{m}$ and $v_{\max} = 30\text{m/s}$ and the corresponding triangular fundamental diagram.

During the simulation time, the leading CAV tries to maintain at an equilibrium speed but it encounters sinusoidal disturbance, which is similar to [83]. The equilibrium speed is $v_0 = 15\text{m/s}$ and the equilibrium headway is $h = 22\text{m}$. And if we denote p as the duration of each period of the sinusoidal disturbance and A as the amplitude of the disturbance, then the velocity of the leading vehicle can be written as:

$$v_N = v_0 + A \sin\left(\frac{2\pi}{p} t\right), \tag{2.20}$$

where the periods are set to $p = 5,\ 10,\ 15,\ 20$s, with an amplitude $A = 5$m/s. OVM and P-OVM with sensitivity constant $a = 1.2,\ 2.4$ are tested with a simulation duration is 60 seconds for all cases. Simulation results are shown in Figures 2.14-2.17. Figure 2.14, 2.15 are the headway profiles of OVM and P-OVM with sensitivity constant $a = 1.2$ under different perturbation frequency. Figure 2.16, 2.17 are the headway profiles of OVM and P-OVM with sensitivity constant $a = 2.4$ under different perturbation frequency. To further show the difference in the P-OVM cases, Table 2.1 presents the average oscillations across all vehicles for various sensitivity constants and perturbations.

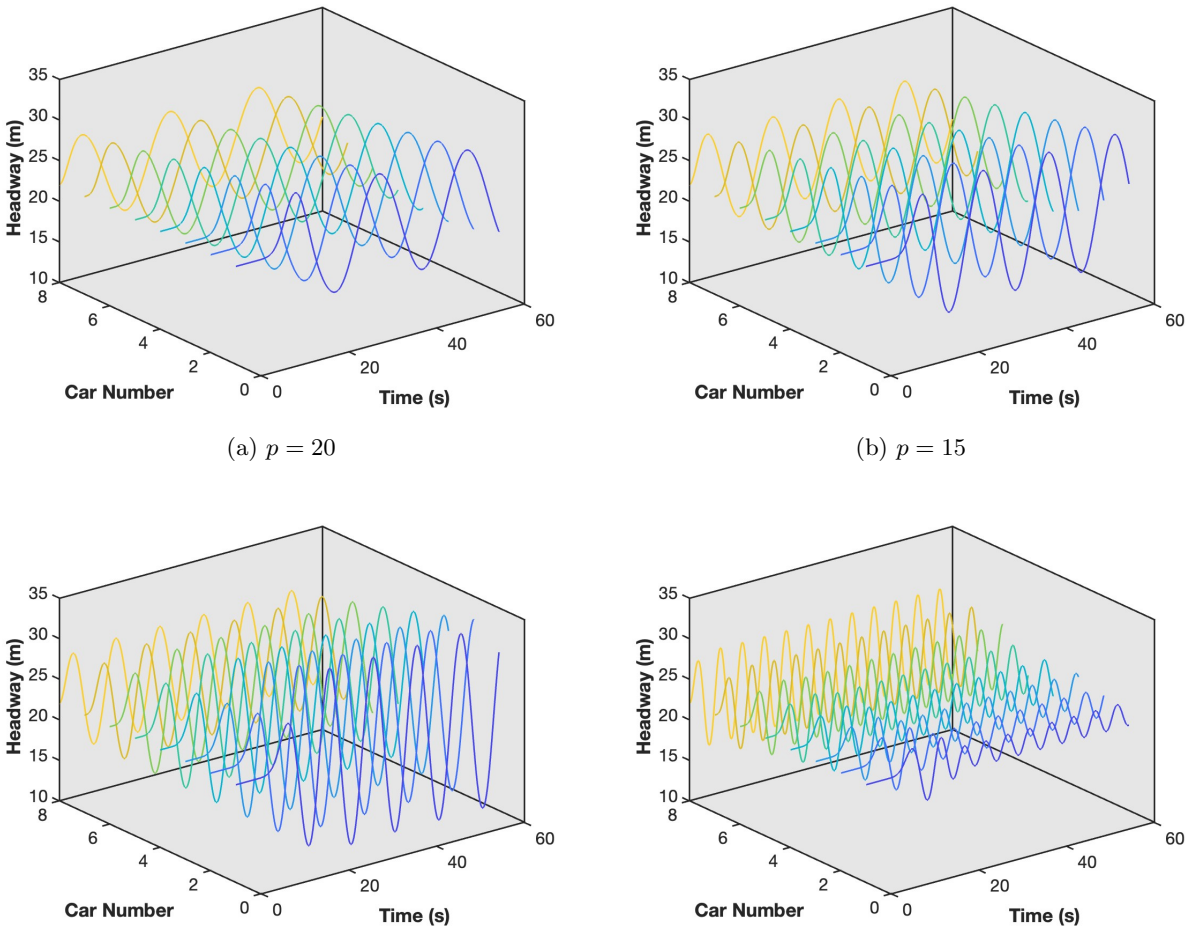

(a) $p = 20$

(b) $p = 15$

(c) $p = 10$

(d) $p = 5$

FIGURE 2.14. Headway profile of OVM with sensitivity constant $a = 1.2$ and period parameter $p = 5,\ 10,\ 15,\ 20$

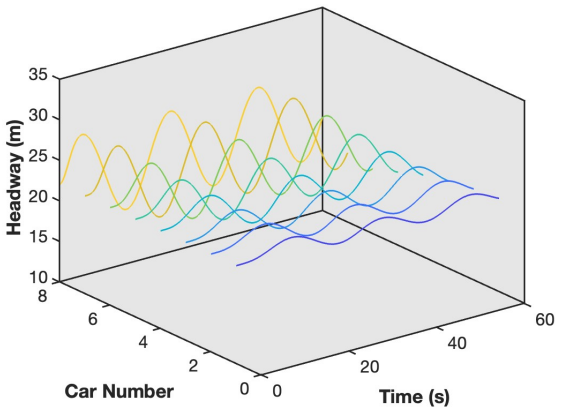

(a) $p = 20$

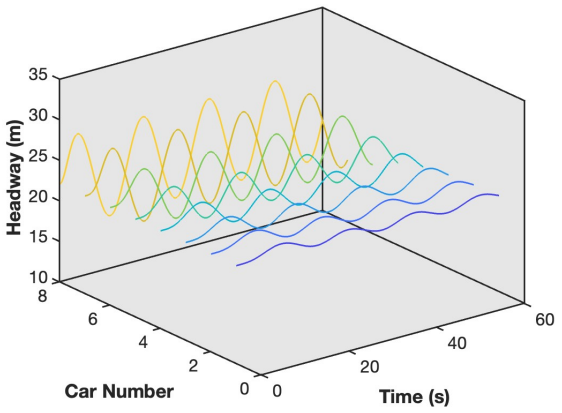

(b) $p = 15$

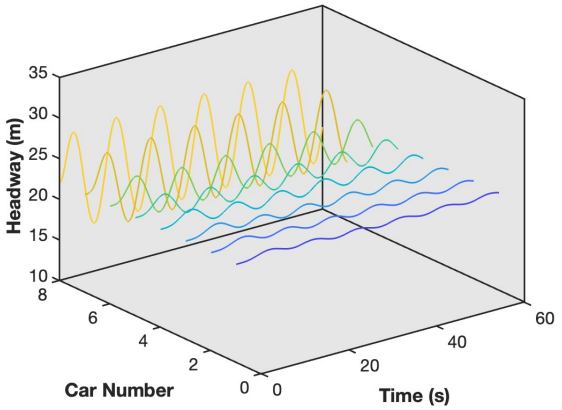

(c) $p = 10$

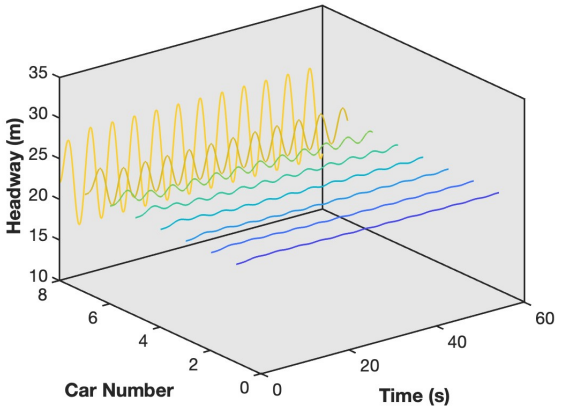

(d) $p = 5$

FIGURE 2.15. Headway profile of P-OVM with sensitivity constant $a = 1.2$ and period parameter $p = 5,\ 10,\ 15,\ 20$

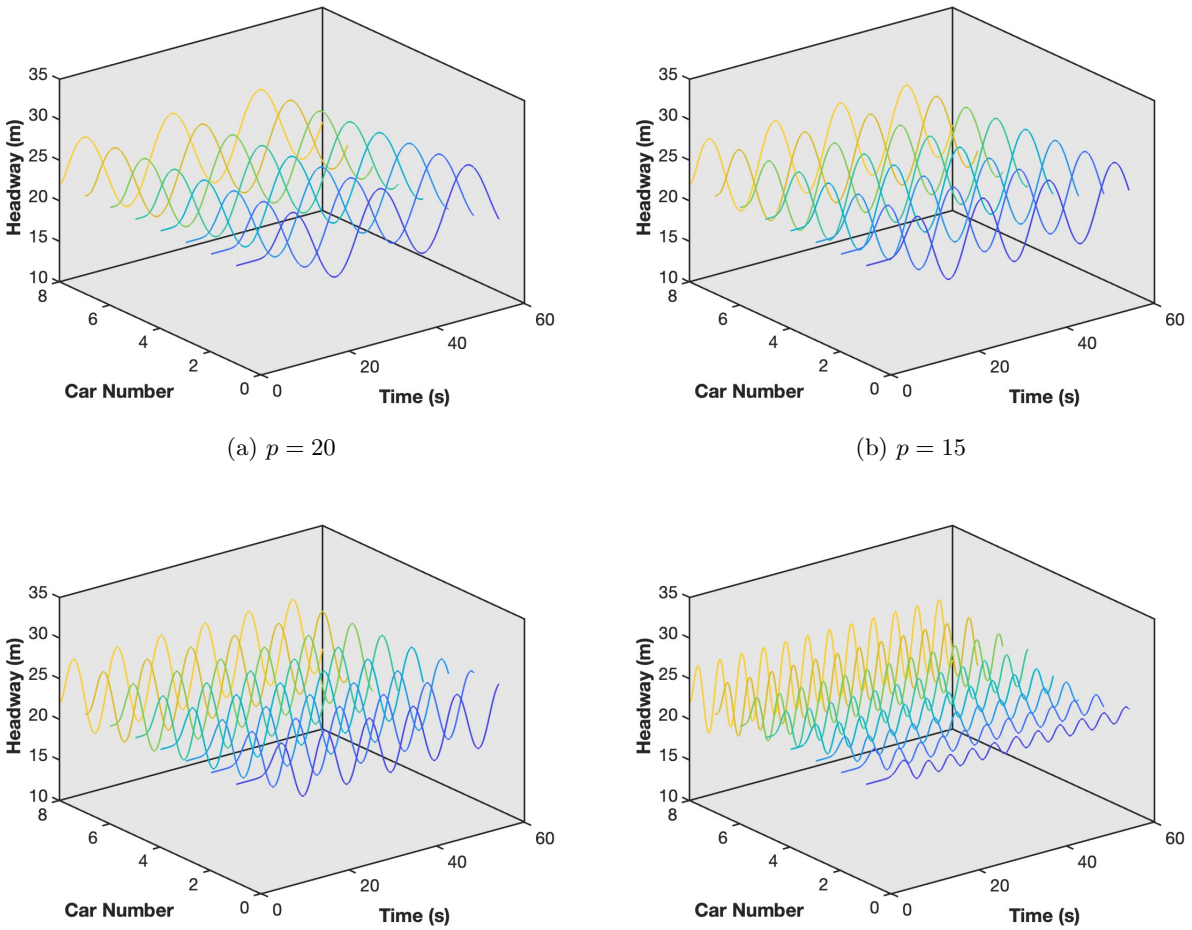

(a) $p = 20$

(b) $p = 15$

(c) $p = 10$

(d) $p = 5$

FIGURE 2.16. Headway profile of OVM with sensitivity constant $a = 2.4$ and period parameter $p = 5,\ 10,\ 15,\ 20$

sensitivity/period	$p = 5$	$p = 10$	$p = 15$	$p = 20$
$a = 1.2$	0.5055m	0.8966m	1.1276m	1.3279m
$a = 2.4$	0.4256m	0.7382m	0.9882m	1.2049m

TABLE 2.1. The average oscillations (in meters) across all vehicles for sensitivity constant $a = 1.2,\ 2.4$ and period parameter $p = 5,\ 10,\ 20,\ 30$

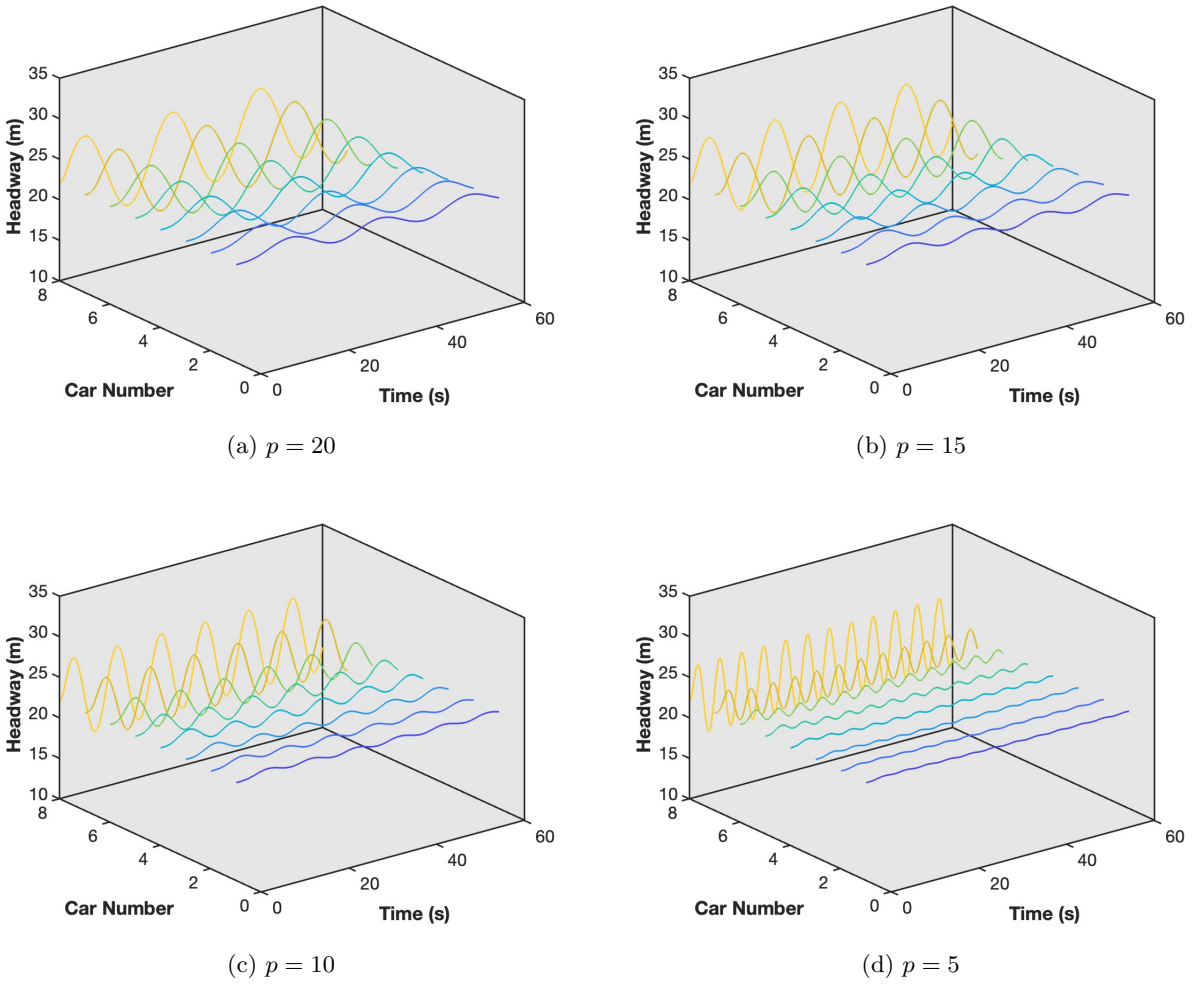

(a) $p = 20$

(b) $p = 15$

(c) $p = 10$

(d) $p = 5$

FIGURE 2.17. Headway profile of P-OVM with sensitivity constant $a = 2.4$ and period parameter $p = 5,\ 10,\ 15,\ 20$

From the simulation results, we observe that when the frequency of the sinusoidal disturbance is high ($p = 5$), the disturbance amplitude can decrease even without platoon control, despite the OVM being unstable at $a = 1.2$. This is possibly due to the frequent changes of the optimal velocity and the delayed reaction inherent in OVM. However, with the P-OVM, the headways

stabilize around the equilibrium state for all vehicles, and the oscillations are smaller. Stability improves slightly for $a = 2.4$ compared to $a = 1.2$, suggesting that a high level of sensitivity is not necessary for CAVs. In summary, P-OVM enhances string stability under periodic disturbances.

2.5. Conclusions

In this chapter, we introduced two models: a platoon model with a coordinated following strategy (P-OVM) and a transition phase model with adjustable parameters (T-OVM). While P-OVM was theoretically proven to be always linearly stable, its practical application may be constrained by safety concerns when both control and state measurements are prone to errors. We also analyzed the stability of the base and transition phase models, providing conditions for their stability. To verify the theoretical findings, numerical simulations were performed on both a ring road with an initial disturbance and an infinite road with periodic disturbances. Several model parameters were tested and analyzed. The simulation results confirmed that the proposed platoon control guarantees linear stability for all sensitivity constants, with the constants influencing how quickly disturbances are attenuated within the platoon. For the transition phase model, with a fixed total sensitivity, stability improved with increased sensitivity to the leading vehicle, in line with theoretical predictions.

The proposed P-OVM and T-OVM significantly outperformed the HDVs' model (OVM) in suppressing disturbances and maintaining string stability. These models are simple forms of platooning that multi-following models tend to focus on, representing a significant improvement over previous multi-following models. With the rapid development of CAV technologies, the proposed platoon control strategy offers a promising solution for mitigating traffic oscillations.

This chapter can be extended in various directions for future research, including: (1) incorporating communication delays into the proposed models and analyzing their impact on stability; (2) extend the proposed models to multiple CAV platoons with interactions; (3) examining more complex road conditions, such as multi-lane ring roads with mixed CAVs and HDVs, with adjustments to the control design for the leading vehicle; (4) conducting field experiments with CAVs to test the proposed control design under various traffic and road conditions.

CHAPTER 3

ODE models: CF models for multiple CAV platoons

3.1. Introduction

In this chapter we start with reviewing studies related to adaptive cruise control (ACC), as the CF related papers have already been discussed in detail in Chapter 2.

Control strategies for groups of CAVs, particularly ACC and Cooperative Adaptive Cruise Control (CACC), have been extensively studied to improve vehicle platooning efficiency and safety [40, 65]. ACC primarily focuses on maintaining safe distances between vehicles by adjusting speed based on sensor data, achieving better results than typical human drivers. However, it operates in a decentralized manner without relying on vehicle-to-vehicle (V2V) communication. On the other hand, CACC utilizes V2V communication to enable more precise control and coordination among CAV platoons [4, 55, 79]. Additionally, the quality of communications plays a crucial role in the stability of CAV platoons, as shown in studies on robust communication and stability analysis [13, 73, 74]. These studies highlight the advantages of CACC over ACC, particularly regarding communication and coordination within platoons.

Beyond ACC and CACC, advanced control strategies such as Model Predictive Control (MPC), reinforcement learning (RL), and stochastic optimization have been explored to further improve the performance of CAVs in complex traffic scenarios. Several related papers are reviewed in chapter 2.

Despite the growing trend of investigating the stability of longitudinal interactions among multiple CAV platoons, few studies have explored their implications using ODE-based CF models or in mixed traffic scenarios involving HDVs. To address this research gap, this chapter propose a foundational framework for multiple platoons of CAVs that is adaptable to various CF models and control designs. We extend a recently proposed single-platoon CF model [21] to a multi-platoon model that accommodates different control strategies and communication capabilities between platoons. Particularly, when the platoon sizes are set uniformly to one, the model degenerates to a classic

CF model for HDVs, or AVs equipped with backward detection. Theoretically, we demonstrate that the stability of the multi-platoon models depends on the platoon size and communication level: larger platoon sizes and enhanced communication contribute to increased stability, while minimal delays between platoons have a negligible effect on stability. Numerical simulations on a ring road, involving different vehicle arrangements and mixed traffic scenarios with various sizes of CAV platoons and HDVs in different ratios and orders, support our theoretical findings. The simulation results also demonstrate that HDVs benefit from following CAV platoons, even when the CAV platoons are not specially designed to control the HDVs.

The remaining part of this chapter is organized as follows. In 3.2, we introduce the CF models for single and multiple platoons of CAVs. In 3.3, stability criteria of the proposed models are presented and proved. In section 3.4, we perform numerical simulations for the proposed models with various traffic assignments on a ring road. The impact of delay and connectivity are analysed. Lastly in section 3.5, conclusion and possible extensions are given.

3.2. Models for CAV platoons

3.2.1. General assumptions. We assume that there are m CAV platoons on a single lane road with no overtaking allowed, where $m \geq 1$. The m-th platoon is the leading platoon, and N_i denotes the size of the i-th platoon. Within the i-th platoon the N_i-th car is the leading vehicle. Moreover, if the single lane road is a ring road, the m-th platoon is following the 1st platoon.

We select the commonly used Optimal Velocity Model (OVM) [3] as the base CF model for human driven vehicles (HDVs). The OVM is expressed as

$$\ddot{x}_i(t) = a\left[V(x_{i+1}(t) - x_i(t)) - \dot{x}_i(t)\right], \tag{3.1}$$

where $x_i(t)$, $i = 1, 2, \ldots N$ is the position of i-th vehicle at time t. $x_{i+1}(t) - x_i(t) \triangleq h_i(t)$ represents the spatial headway between the i-th and $i+1$-th vehicle. $\dot{x}_i(t)$, $\ddot{x}_i(t)$ denotes the velocity and acceleration of the i-th vehicle at time t, respectively. $V(h)$ is the optimal velocity function of headway (head to head distance) h, and a is a sensitivity constant. An example of optimal velocity

function is as follows:

$$V(h) = \begin{cases} v_f, & \text{if } h \geq h_f; \\ \frac{v_f}{2}\left(1 - \cos\left(\pi \frac{h-h_s}{h_f-h_s}\right)\right), & \text{if } h_s \leq h \leq h_f; \\ 0, & \text{if } h \leq h_s, \end{cases} \tag{3.2}$$

where h_s is the standstill headway, h_f is the free flow headway, v_f is the free flow speed and l is the length of each vehicle. This is equivalent to the function in [67]. Figure 3.1 is an example plot of (3.2) and the corresponding fundamental diagram (density-flow diagram) as in [21].

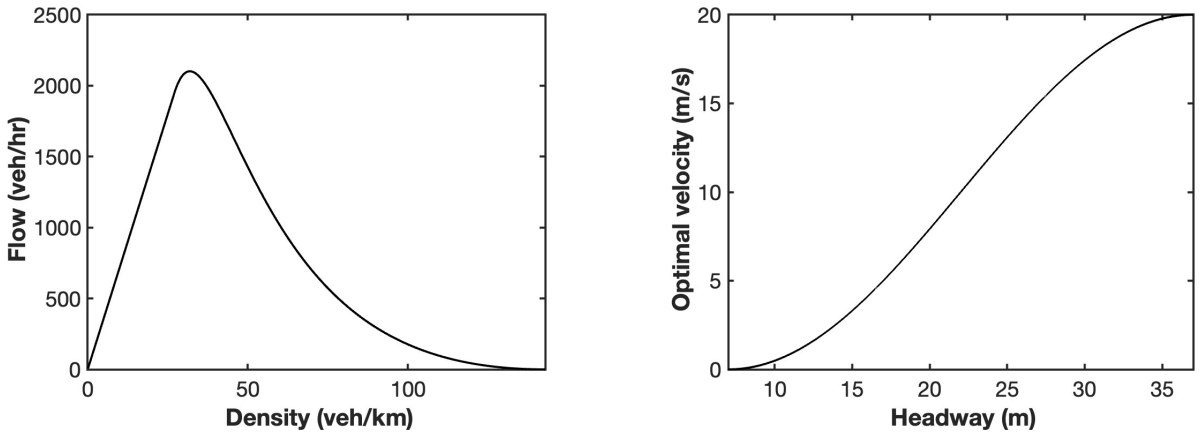

(a) Optimal velocity function

(b) Fundamental diagram

FIGURE 3.1. Plot of an optimal velocity function and the corresponding fundamental diagram.

3.2.2. Single platoon: base model. Before investigating multi-platoon models, it is essential to develop a robust single-platoon CF model. In [21], it is shown that if a platoon is sufficiently close to its equilibrium state, the platoon controlled OVM (P-OVM) is always stable under small initial disturbances and periodic disturbances. The proposed model is of the form

$$\ddot{x}_i(t) = a\left[V(\frac{x_N(t) - x_i(t)}{N-i}) - \dot{x}_i(t)\right], \; i = 1, 2, \ldots, N \tag{3.3}$$

where N represents the platoon size, and x_N is the position of the controlled leading vehicle. Figure 3.2 is a visual interpretation of this model.

However, the reliability of (3.3) assumes that platoon followers can precisely acquire information from the leading vehicle with no delay, which is unrealistic for a large number of CAVs. Therefore,

FIGURE 3.2. CF pattern of a single platoon

a multi-platoon system (where one platoon follows annother) serves as a viable formation strategy for managing long strings of vehicles, helping to mitigate the effects of communication delays and instabilities in centralized controls. In the following subsections, we provide some examples of multi-platoon models where we assume that each platoon is governed by (3.3) and the speed of platoon leaders are controlled as inputs. We will neglect the effects of communication delays and minor adjustments within each platoon.

3.2.3. Multi-platoon: no inter-connection . If there is no communication between platoons, we assume that the leading vehicle of each platoon only follows the last vehicle of the platoon ahead, as shown in Figure 3.3. If no additional control is applied, the platoon leaders are directly

FIGURE 3.3. CF pattern of multiple platoons with no inter-platoon communication.

following the vehicle ahead according to the OVM:

$$\ddot{x}_{i,N_i} = a(V(x_{i+1,1} - x_{i,N_i}) - \dot{x}_{i,N_i}), \tag{3.4}$$

where $1 \le i \le m-1$. For the followers within each platoon, the centralized platoon controller (3.3) is applied:

$$\ddot{x}_{i,j} = a\left[V\left(\frac{x_{i,N_i} - x_{i,j}}{N_i - j}\right) - \dot{x}_{i,j}\right], \tag{3.5}$$

where $1 \le i \le m$ and $1 \le j \le N_i - 1$. In particular, if we have platoon size $N_m = 1$ or 2 for all m, the proposed model reduces to the OVM for HDVs.

3.2.4. Multi-platoon: two-way inter-connection . In this subsection we suppose each platoon can communicate with platoons ahead and behind, with some delays (i.e. the platoons are two-way connected), as shown in Figure 3.4. In this case, we can model the platoon leaders to

FIGURE 3.4. CF pattern of multiple platoons with forward and backward inter-platoon communication.

follow both the platoon leader in front and the one behind, similar to the model for autonomous vehicles proposed in [85]:

$$\ddot{x}_{i,1} = a\left[(1+p)V\left(\frac{\Delta_i(t-t_d)}{N_i}\right) - pV\left(\frac{\Delta_{i-1}(t-t_d)}{N_{i-1}}\right) - \dot{x}_{i,1}\right], \tag{3.6}$$

where $\Delta_i(t) = x_{i+1,1}(t) - x_{i,1}(t)$ is the headway between the i-th and $i+1$-th platoon leader, p is the smoothing factor for the platoon in the back, and t_d is the constant communication delay between platoons. For the followers we apply the same equation (3.5) as in the previous model. In particular, if the platoon size $N_m = 1$ and $t_d = 0$ for all m, (3.6) becomes equivalent to the modified OVM with autonomous vehicles in [85].

REMARK 3.2.1. *The proposed frame work can be applied to any general second order CF models and combined with control strategies such as delayed feedback control, CACC, MPC, etc. However, the main focus of this chapter is to present a basic framework for multi-platoon CAVs, so we have kept the models as simple as possible with minimal parameters.*

3.3. Stability analysis

In this section, we analyse the stability of the models in section 3.2 through linear stability analysis. The steady-state (equilibrium) solution of all the aforementioned models on a ring road of length L with $N_{tot} = \sum_{i=1}^{m} N_i$ vehicles is

$$e_{i,j}(t) = h(N_1 + \cdots + N_{i-1} + j) + V(h)t, \tag{3.7}$$

where $h = L/N_{tot}$ is the equilibrium headway. To analyse the effect of platoon sizes, for the stability analysis we assume that for the multi-platoon models all the platoons are of a uniform size, denoted as N. Then for the no-connection model proposed in Subsection 3.2.3, the following stability criterion holds:

THEOREM 3.3.1. *The no-connection multi-platoon model (3.4, 3.5) with identical platoon size N is stable if*

$$a > \frac{2NV'(h)}{(N-1)^2+1}. \tag{3.8}$$

PROOF. Assume that for each vehicle there is a small deviation from the equilibrium solution:

$$x_{i,j}(t) = e_{i,j}(t) + y_{i,j}(t),\ |y_{i,j}| \ll 1. \tag{3.9}$$

Since the platoon leader is just following the last vehicle of the platoon in front, for the first and last vehicle of each platoon they formulate an sub-system of ODEs of $2m$ equations. And we can linearize the sub-system by doing Taylor expansion of $y_{i,j}$ and neglect higher order terms to get

$$\ddot{y}_{i,N}(t) = a\left[V'(h)(y_{i+1,1}(t) - y_{i,N}(t)) - \dot{y}_{i,N}(t)\right] \tag{3.10}$$

for platoon leaders, and

$$\ddot{y}_{i,1}(t) = a\left[V'(h)\frac{y_{i,N}(t) - y_{i,1}(t)}{N-1} - \dot{y}_{i,1}(t)\right] \tag{3.11}$$

for the platoon tails, where i is referring to all the integers that satisfies $1 \le i \le m$ throughout the proof. The $(m+1)$-th platoon is the same as the 1st platoon. Then if λ is an eigenvalue of the linear ODE system, and $\xi_{i,j}$ are the corresponding coefficients of $y_{i,j}$, simplified from (3.11, 3.10) we have

$$\lambda^2 + a\lambda - aV'(h)\left(\frac{\xi_{i+1,1}}{\xi_{i,N}} - 1\right) = 0, \tag{3.12}$$

and

$$\lambda^2 + a\lambda - aV'(h)\left(\frac{\xi_{i,N}}{(N-1)\xi_{i,1}} - \frac{1}{N-1}\right) = 0. \tag{3.13}$$

Then with the same λ, the constant parts of (3.12) and (3.13) are identical, and we can denote it by r. Then the real parts of λ can be rewritten as

$$\mathrm{Re}(\lambda) = \frac{1}{2\left(-a + \sqrt{(\frac{d+\sqrt{d^2+e^2}}{2})}\right)}, \tag{3.14}$$

where $d = a^2 + 4\mathrm{Re}(r)$ and $e = 4\mathrm{Im}(r)$. The sub-system (3.11, 3.10) is stable if $\mathrm{Re}(\lambda) < 0$, which can be simplified to

$$a > \left|\frac{\mathrm{Im}^2(r)}{\mathrm{Re}(r)} V'(h)\right|. \tag{3.15}$$

Now it remains to show (3.8) implies (3.15). Note that

$$\prod_{i=1}^{m} \frac{\xi_{i+1,1}}{\xi_{i,N}} \frac{\xi_{i,N}}{\xi_{i,1}} = 1 \tag{3.16}$$

holds since $m + 1 = 1$ on the ring road, combining with (3.12, 3.13) we have r satisfies

$$((N-1)r + 1)^m (r+1)^m = 1. \tag{3.17}$$

Then we can solve for r to get

$$r = \frac{-N \pm \sqrt{N^2 - 4(N-1)(1 - \exp(\frac{2\pi k i}{m}))}}{2(N-1)}, \tag{3.18}$$

where $k = 1, 2, \ldots, m$. Let $\theta = \frac{2\pi k}{m}$ and $l = 1/(N-1)$, then

$$-\frac{\mathrm{Im}^2(r)}{\mathrm{Re}(r)} = \frac{\sqrt{d_2^2 + e_2^2} - d_2}{l + 1 \pm \sqrt{\frac{\sqrt{d_2^2+e_2^2}+d_2}{2}}}, \tag{3.19}$$

where $d_2 = (l+1)^2 - 4l(1-\cos\theta)$ and $e_2 = 4l\sin\theta$. Therefore (3.19) can be considered as a function of θ, and for $l < 1$ this is a decreasing function for $\theta > 0$. Then we can obtain

$$\left|\frac{\mathrm{Im}^2(r)}{\mathrm{Re}(r)}\right| < \lim_{\theta \to 0^+} \left(-\frac{\mathrm{Im}^2(r)}{\mathrm{Re}(r)}\right) = \frac{2N}{(N-1)^2 + 1}. \tag{3.20}$$

Combined (3.20) with (3.15), the sub-system (3.11, 3.10) is stable if the stability criterion (3.8) holds. For the remaining vehicles inside each platoon, the solution is only determined by the leading

vehicle of the platoon. And by linearization of (3.5) we can rewrite $y_{i,j}$ as

$$y_{i,j} = \left(N - j + \frac{j-1}{N-1}\right) y_{i,N}, \tag{3.21}$$

which is a linear function of $y_{i,N}$. This means the stability of the multi-platoon system is the same as the sub-system (3.11, 3.10). Therefore stability criterion (3.8) holds. □

Figure 3.5 is the plot of stability regions with different platoon size of the no-connection model.

REMARK 3.3.1. *For all the stability plots, each neutral stability line separates the graph into two regions: the region above the line is stable and the region below the line is unstable.*

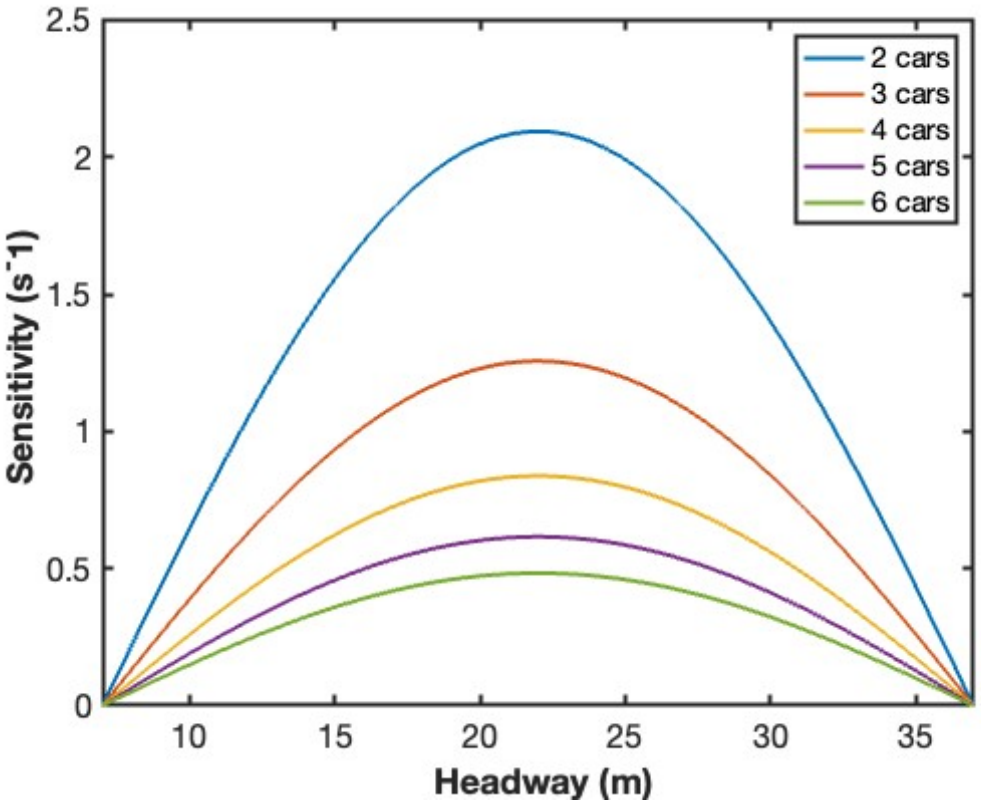

FIGURE 3.5. Neutral stability lines of the multi-platoon model with no connection of platoon size $N = 2, 3, 4, 5, 6$.

Using similar approaches, for the two-way connected model proposed in Subsection 3.2.4, the following stability criterion applies:

THEOREM 3.3.2. *The two-way connected multi-platoon model (3.6, 3.5) with identical platoon size N is stable if*

$$a > \frac{2V'(h)}{(1+2p)(N-2t_dV'(h))}. \tag{3.22}$$

PROOF. For the connected model (3.6, 3.5) we follow the assumptions of previous works, e.g. [47, 80] such that higher orders of the constant delay t_d are neglected. And after linearization, for the connected multi-platoon system in Subsection 3.2.4, The m platoon leaders form a system of m linear ODEs:

$$\ddot{y}_{i,N}(t) = a\left[V'(h)(1+p)\frac{\Delta_{i,N}(t-t_d)}{N} - V'(h)p\frac{\Delta_{i-1,N}(t-t_d)}{N} - \dot{y}_{i,N}(t)\right]. \tag{3.23}$$

Then if λ is an eigenvalue of the system, by reserving first order of t_d via Taylor expansion, we have

$$\lambda^2 + a(1+2p)\lambda - (1-\lambda t_d)\frac{aV'(h)}{N}(1-e^{i\theta}) = 0, \tag{3.24}$$

where θ is the same as in the proof of Theorem 3.3.1. Then by simplifying the condition $\mathrm{Re}(\lambda) < 0$, the stability criterion is equivalent to

$$4k(1-\cos\theta) + 8at_dk^2(1-\cos\theta)^2 > k^2\sin^2\theta, \tag{3.25}$$

where $k = a/(N \cdot V'(h))$. Then let $\theta \to 0$ we can get the stability criterion given in Theorem 3.3.2. □

Figure 3.6 is the plot of the front connected model's stability regions ($p = 0, t_d = 0$). We observe that the connected model exhibits larger stability regions than the non-connected model. However, the difference diminishes as platoon size increases. Figure 3.7 is the plot of the two-way connected model's stability regions with different delays of backward sensitivity $p = 0.3$ and platoon size $N = 4$. From this figure, we can observe that the effect of delay become larger as it get close to 1.6s. Additionally, if the delay reach 2s then the model becomes consistently unstable for headways between 20 and 25 meters.

REMARK 3.3.2. *For the effect of backward sensitivity p we refer to [43, 85].*

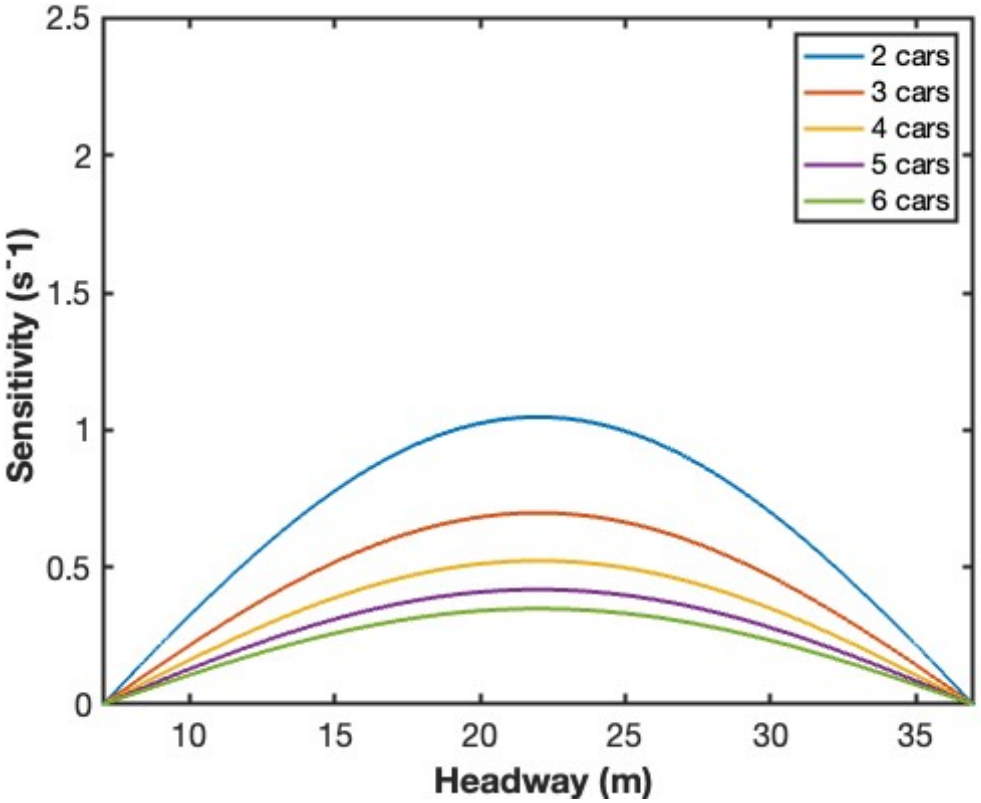

FIGURE 3.6. Neutral stability lines of the multi-platoon model with front connection of platoon size $N = 2, 3, 4, 5, 6$ and zero-delay.

3.4. Numerical simulations

3.4.1. General information. We use MATLAB 2024a for both simulation and plots. All the simulations are performed on a single-lane ring road. To acquire more realistic results, we modified the OVM by adding a maximum acceleration constraint and an emergency braking system as follows:

- Maximum acceleration constraint: Due to mechanical limits, the maximum allowable acceleration can be less than the theoretical value predicted by the optimal velocity model. For the simulations in this section, we add a constant maximum acceleration constraint, denoted as a_m.
- Emergency braking system: To avoid collisions, we implement an emergency braking system. If the headway of two adjacent vehicles get smaller than the safety headway h_m

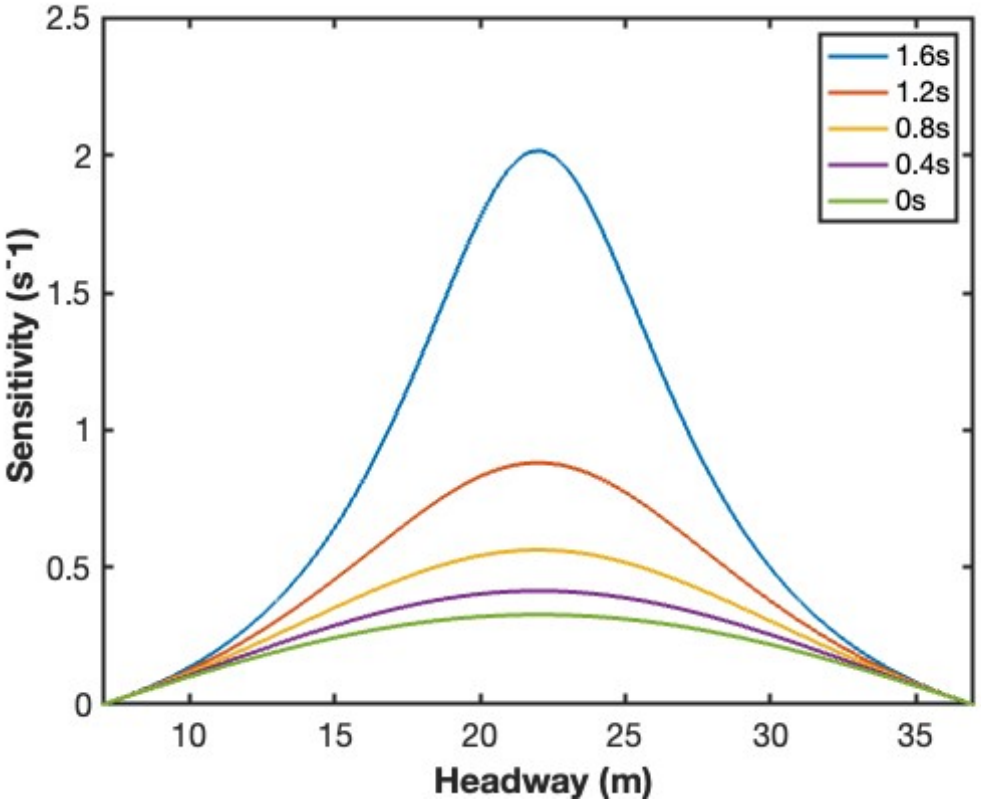

FIGURE 3.7. Neutral stability lines of the multi-platoon model with two-way connection of platoon size $N = 4$ and delay $t_d = 0, 0.4, 0.8, 1.2, 1.6$s.

(which is a function of the current speed and relative speed between the two vehicles), then the vehicle behind brakes with emergency braking deceleration a_b.

The modified OVM for HDVs is then given by

$$\dddot{\tilde{x}}_i = \begin{cases} \min\left(\ddot{x}_i, a_m\right), \text{ if } x_i(t) - x_{i+1}(t) \geq h_m; \\ a_b, \text{ if } x_i(t) - x_{i+1}(t) < h_m, \end{cases} \tag{3.26}$$

where the acceleration term $\ddot{x}_i$ is given by (3.1).We modify the multi-platoon models accordingly by substituting $\ddot{x}_i$ with other acceleration functions. The solutions of the models are obtained in discrete forms using a modified Euler scheme:

$$\begin{cases} \dot{x}_{i,j+1} = \dot{x}_{i,j} + \dddot{\tilde{x}}_{i,j}\Delta t; \\ x_{i,j+1} = x_{i,j} + \frac{\dot{x}_{i,j} + \dot{x}_{i,j+1}}{2}\Delta t, \end{cases} \tag{3.27}$$

where Δt is the uniform time step size, $x_{i,j}$, $\dot{x}_{i,j}$, $\ddot{\tilde{x}}_{i,j}$ are the position, velocity, acceleration of the i-th car at the j-th time step of simulation, respectively. This scheme is equivalent to the ones in [85] and [21]. We also use a consistent time step size of $\Delta t = 0.1$ seconds.

The model parameters are set as follows: The total length of the ring road is $L = 2640$m, with a total of $N_{tot} = 120$ vehicles. All simulations run for the same duration $T = 4000$ seconds. We set the maximum acceleration constraint to $a_m = 3\text{m/s}^2$, the emergency braking deceleration to $a_b = -8\text{m/s}^2$ and define the safety headway as

$$h_m(v_i, v_{i+1}) = \frac{(v_i - v_{i+1})^2}{|2a_b|} + \tau(v_i - v_{i+1}) + l, \tag{3.28}$$

where v_i is the speed of the i-th vehicle, $\tau = 4$ is the constant time headway for safety, and $l = 5$m is the length of each vehicle. We fix the forward sensitivity as $a = 0.6$ and backward sensitivity as $p = 0.3$ if available. The optimal velocity function is given by equation (3.2), with parameters $h_{\min} = 7$m, $h_{\max} = 37$m, $v_{\max} = 20$m/s. The equilibrium headway and velocity are calculated as $h = L/N = 22$m and $V(h) = 10$ m/s, respectively. The initial position and velocity of the i-th vehicle are deviated from the equilibrium states $(e_i, V(h))$ with random perturbations uniformly distributed on the interval $[-5/2, 5/2]$. The initial condition of the model is given by

$$\begin{cases} x_i(0) = & e_i(0) + r_i, \\ \dot{x}_i(0) = & V(h) + \overline{r}_i \end{cases} \tag{3.29}$$

where $r_i, \overline{r}_i$ are random values generated from a uniform distribution over $[-5/2, 5/2]$, and $e_i(0) = hi$ can be calculated from equation (3.7). In the following subsections, we introduce three sets of simulations involving CAV platoons of varying platoon sizes, communication levels, and distributions in mixed traffic.

REMARK 3.4.1. *For readers interested in variations of sensitivity parameters, studies including [3], [31], [85], [21] explore different sensitivity parameter settings in various simulations.*

3.4.2. Experiments of identical CAV platoons. In this subsection, we conduct experiments on traffic flow consisting solely of identically-sized CAV platoons, aiming to investigate the effects of various factors such as platoon size, connectivity, and communication delay.

3.4.2.1. *Different platoon sizes without delay.* In this simulation, we aim to show the effect of platoon size and connectivity without delay. The platoon sizes are selected as $N = 2, 3, 4, 5$, and the connectivity options between platoons include no-connection, front-connection, and two-way connection. Figure 3.8 is the headway plots for the no-connection model with platoon size $N = 2, 3, 4$ during 3800s to 4000s, and for $N = 5$ from 0s to 200s. In these plots, 20 vehicles are selected at even intervals, starting from the 1st to the 120th vehicle, with every 6th vehicle chosen for representation.

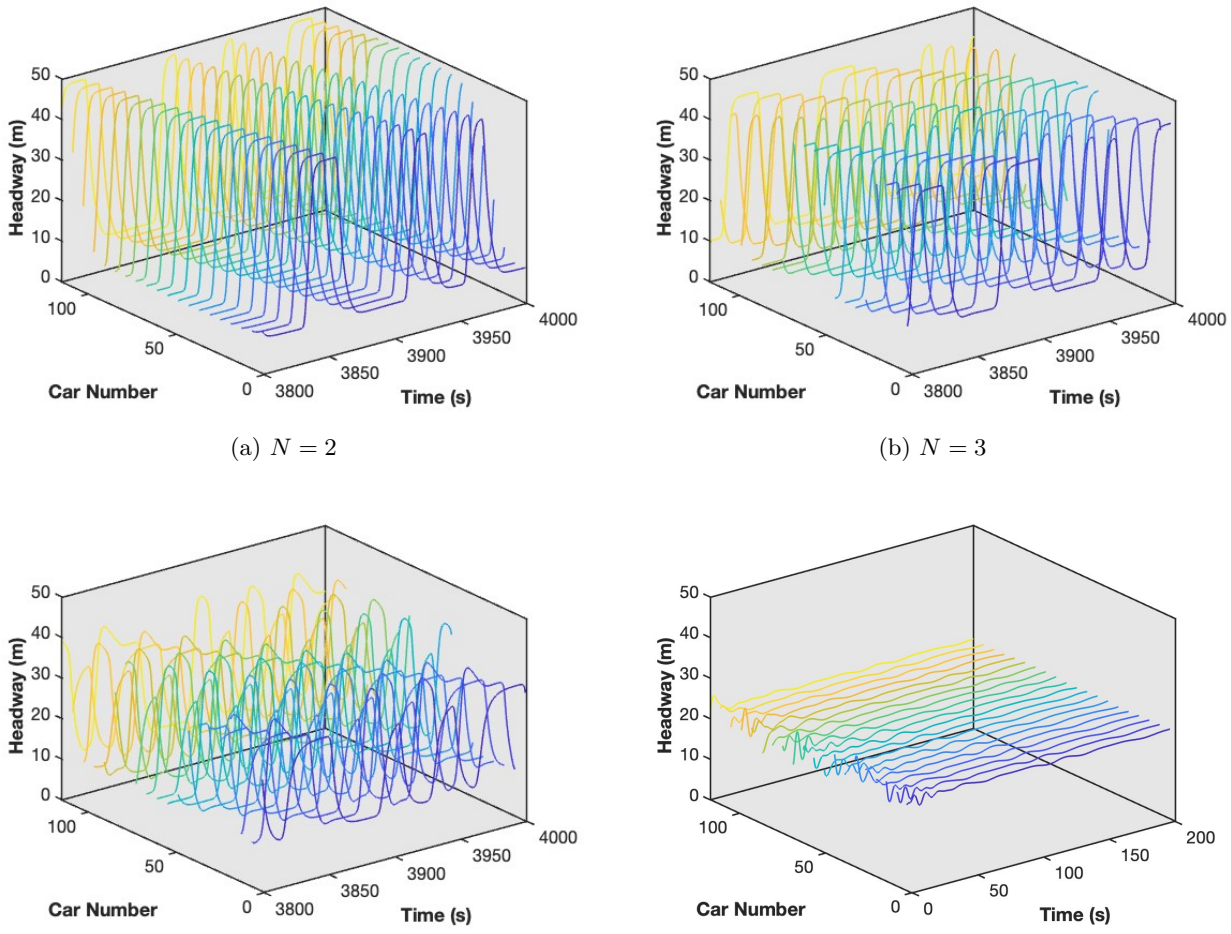

(a) $N = 2$ (b) $N = 3$

(c) $N = 4$ (d) $N = 5$

FIGURE 3.8. Plots of headways for selected vehicles with no-connection for platoon sizes $N = 2, 3, 4, 5$.

REMARK 3.4.2. *For the headway plots in this section, if the vehicles have not stabilized after* 4000*s, we select every 6th vehicle from the 1st to the 120th for plotting, with the time interval*

spanning from 3800 to 4000 seconds. If the vehicles have stabilized, the headway plots will instead cover the time period from 0s until stabilization (60, 200, or 300s, depending on the scenario).

Figure 3.9 is the plots of minimum and maximum speeds of all vehicles corresponding to Figure 3.8. Figure 3.10 is the headway plots for front-connected platoons of size $N = 2, 3, 4$ and for

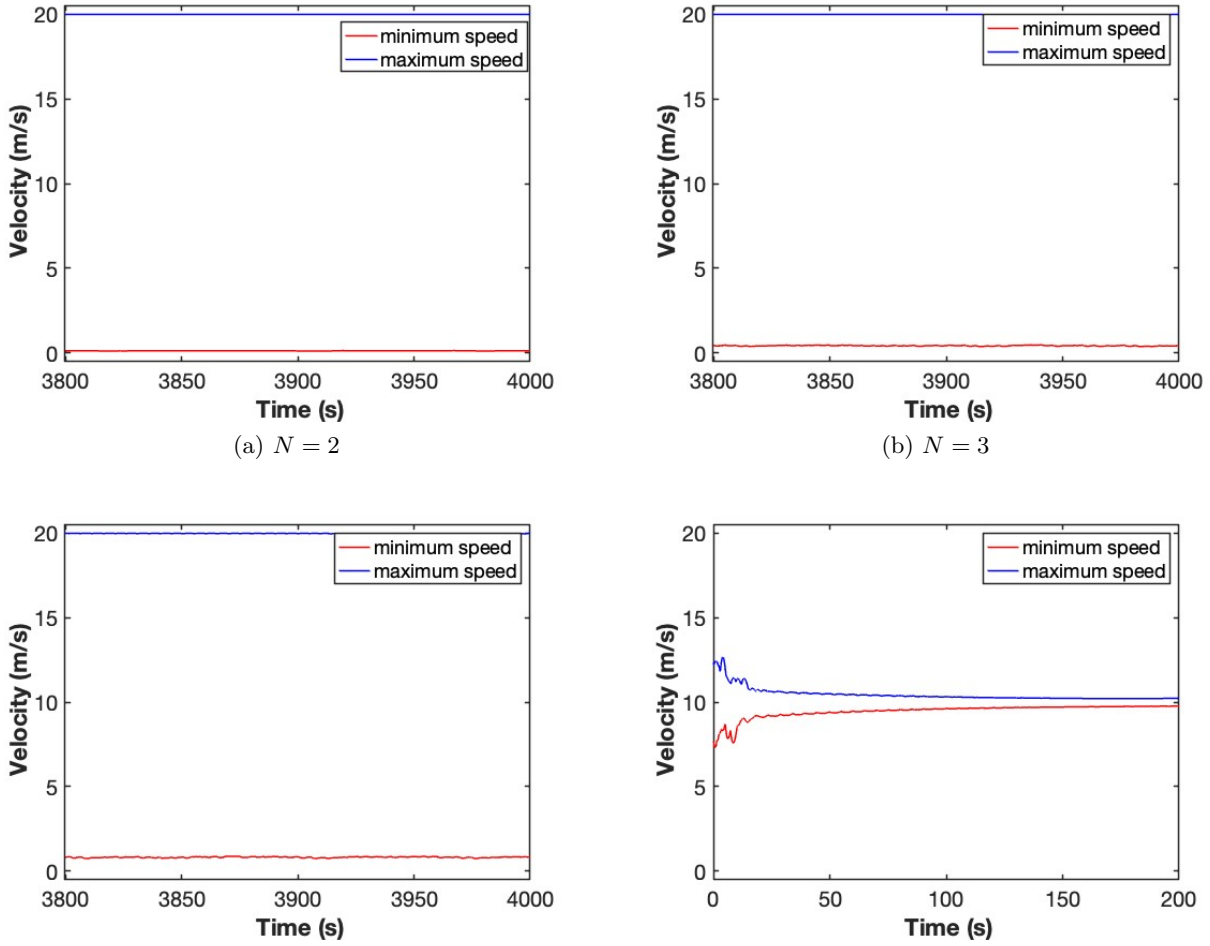

(a) $N = 2$ (b) $N = 3$

(c) $N = 4$ (d) $N = 5$

FIGURE 3.9. Plots of minimum and maximum speeds of platoons with no-connection and size $N = 2, 3, 4, 5$.

two-way connected platoons of size $N = 2$.

From the simulation results, we observe that stability of CAV platoons can be improved by increasing both platoon size and connectivity. Moreover, with two-way connections, the equilibrium state can be achieved with platoons consisting of just two CAVs. However, this condition is only

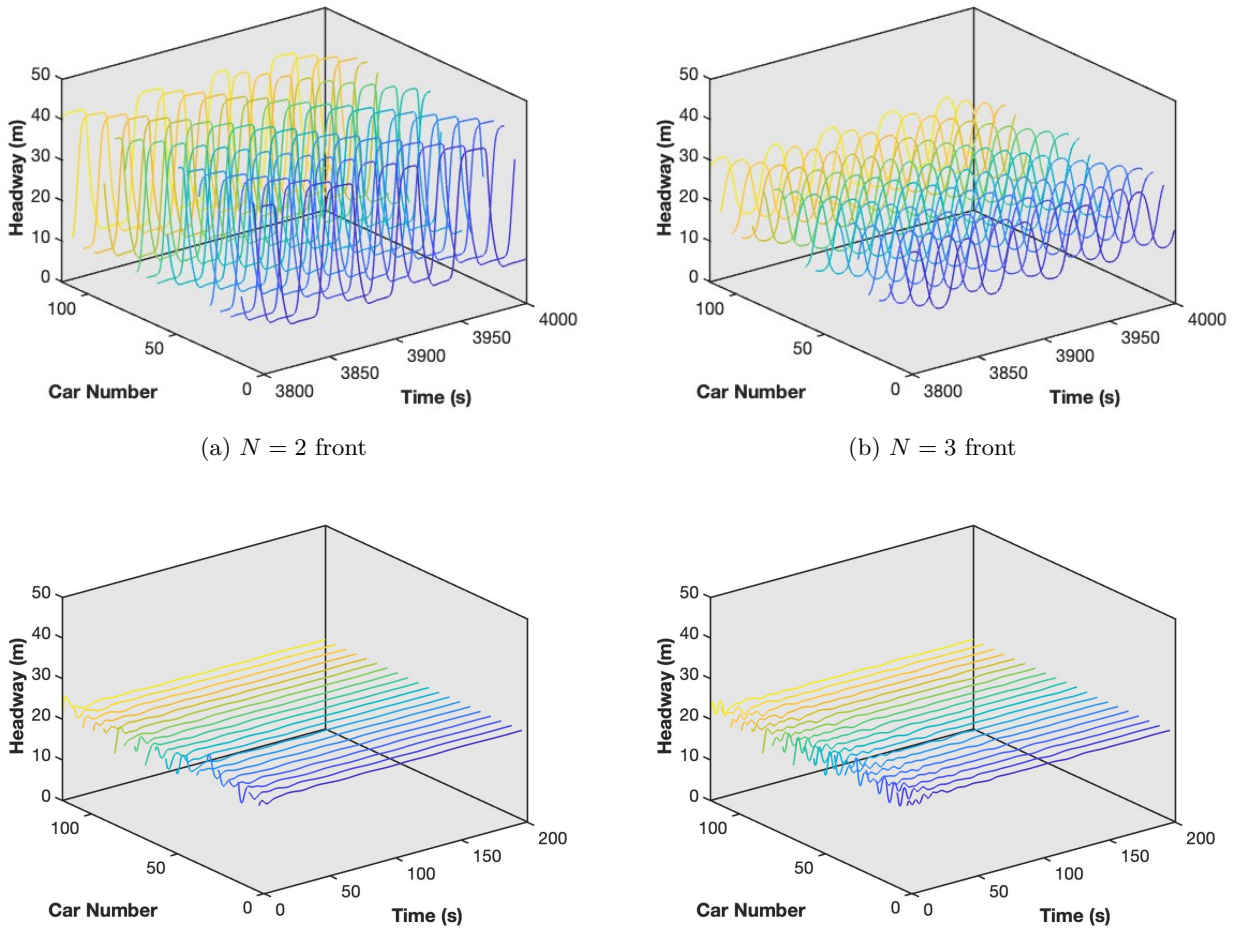

(a) $N = 2$ front

(b) $N = 3$ front

(c) $N = 4$ front

(d) $N = 2$ two-way

FIGURE 3.10. Plots of headways for selected vehicles with front connection for platoon sizes $N = 2, 3, 4$, two-way connection for platoon size $N = 2$.

guaranteed if the intra-platoon connections are robust and the inter-platoon communication is without delay.

3.4.2.2. *Fixed platoon size with different delays.* In this simulation, we aim to find the effects of inter-platoon communication delay. We fix the platoon size at $N = 4$ and select different constant delays for both the front-connected model and two-way connected model. Figure 3.11 is the headway plots for the two-way connected model with communication delays $t_d = 0.4, 0.8, 1.2, 1.6$s. Figure 3.12 is the plots of minimum and maximum speeds of all vehicles corresponding to Figure 3.11.

From the simulation results, we observe that increasing communication delays between platoons negatively impacts the stability of CAV platoons. Moreover, the variance in headways grows

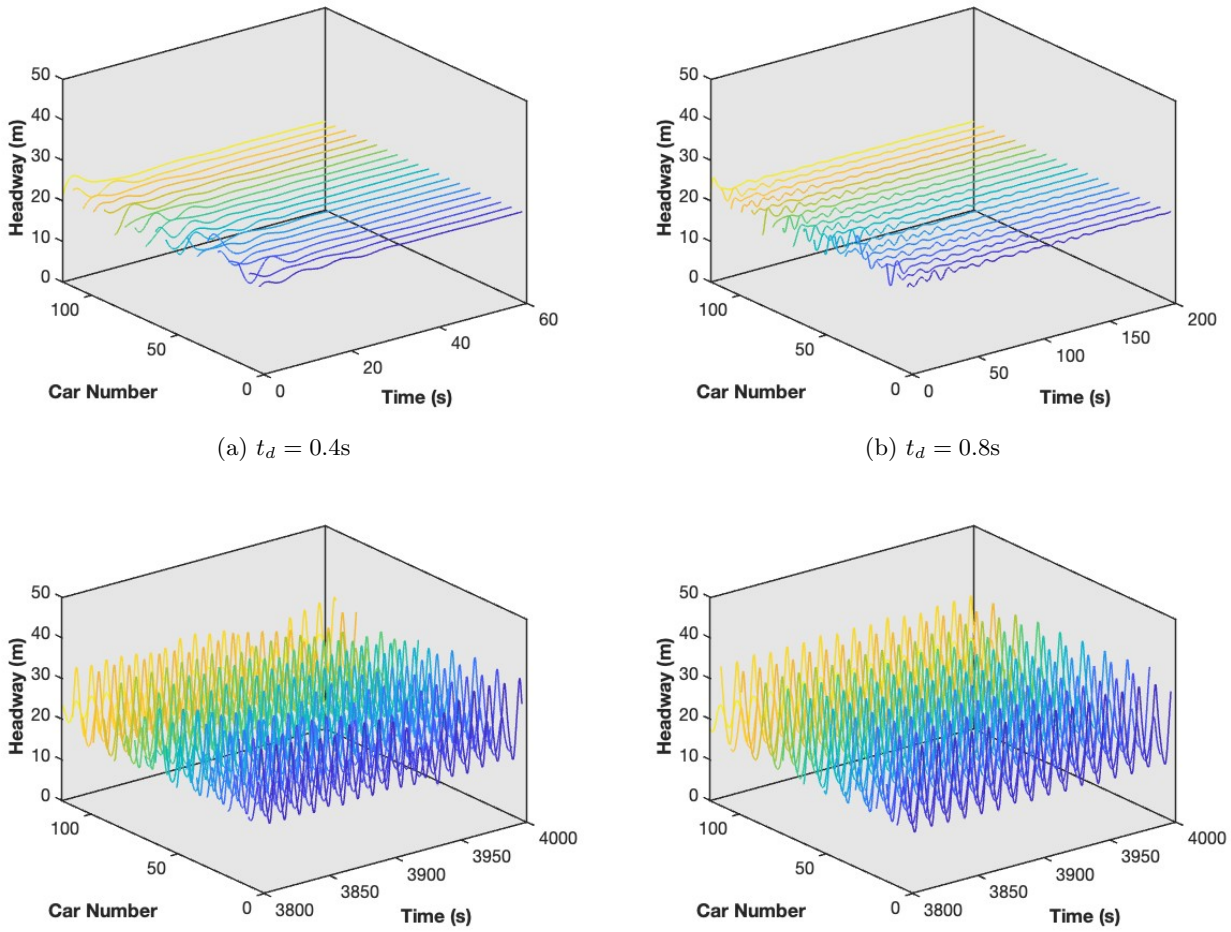

(a) $t_d = 0.4$s

(b) $t_d = 0.8$s

(c) $t_d = 1.2$s

(d) $t_d = 1.6$s

FIGURE 3.11. Plots of headways for selected vehicles with two-way connection for platoon size $N = 4$ and communication delays $t_d = 0.4, 0.8, 1.2, 1.6$s.

exponentially with increased delay, which aligns with theoretical analysis. These findings can guide CAV manufacturers in setting standards for sensors and other hardware components that influence communication delays.

3.4.3. Experiments of CAV platoons mixed with HDVs. One potential benefit of implementing CAV platoons in traffic flow is their stabilizing effect when mixed with HDVs (which can be treated as CAV platoons of size 1 with no communication). In this subsection, we test various distributions of CAV platoons and HDVs on the ring road described in Subsection 3.4.1 to evaluate their impact on traffic flow stability.

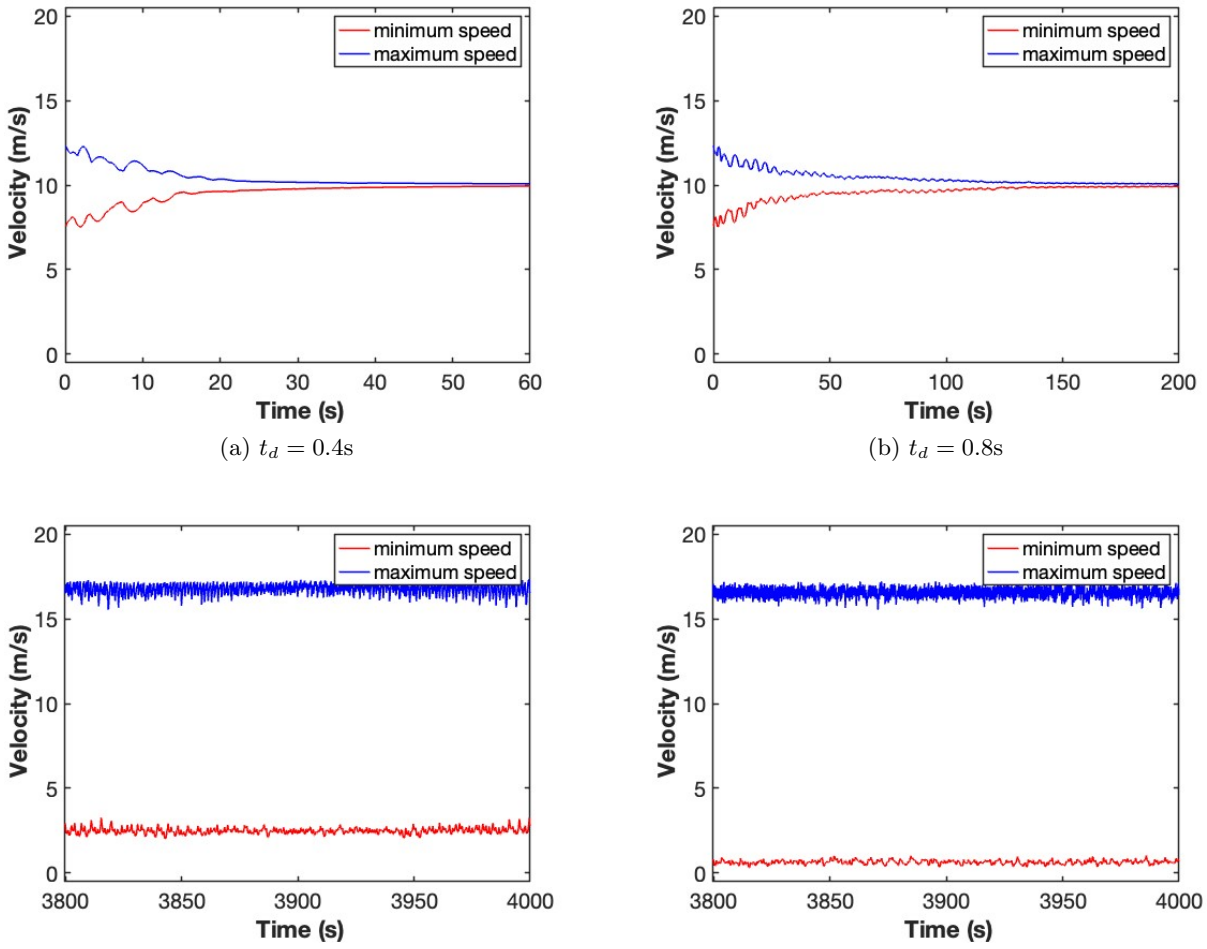

(a) $t_d = 0.4$s (b) $t_d = 0.8$s

(c) $t_d = 1.2$s (d) $t_d = 1.6$s

FIGURE 3.12. Plots of minimum and maximum speeds of platoons with no-connection of size $N = 4$ and communication delays $t_d = 0.4, 0.8, 1.2, 1.6$s.

3.4.3.1. *Segregated CAV platoons and HDVs.* We first consider the scenario where CAV platoons and HDVs are segregated into two distinct groups, each forming its own string of vehicles. The platoon configurations are set with sizes of $N = 6$ or $N = 8$, with no inter-platoon connections. Figure 3.13 is the headway plots for segregated traffic with CAV platoons of size $N = 6$ with either 24 or 30 HDVs, and CAV platoons of size $N = 8$ with either 32 or 40 HDVs.

From this simulation, we observe that platoons of size $N = 6$ can stabilize up to 30 HDVs, slightly less than 32 HDVs stabilized by platoons of size $N = 8$.(It is worth noting that with 40 HDVs, the traffic flow is nearly stable.) Moreover, if the model does not reach equilibrium, the

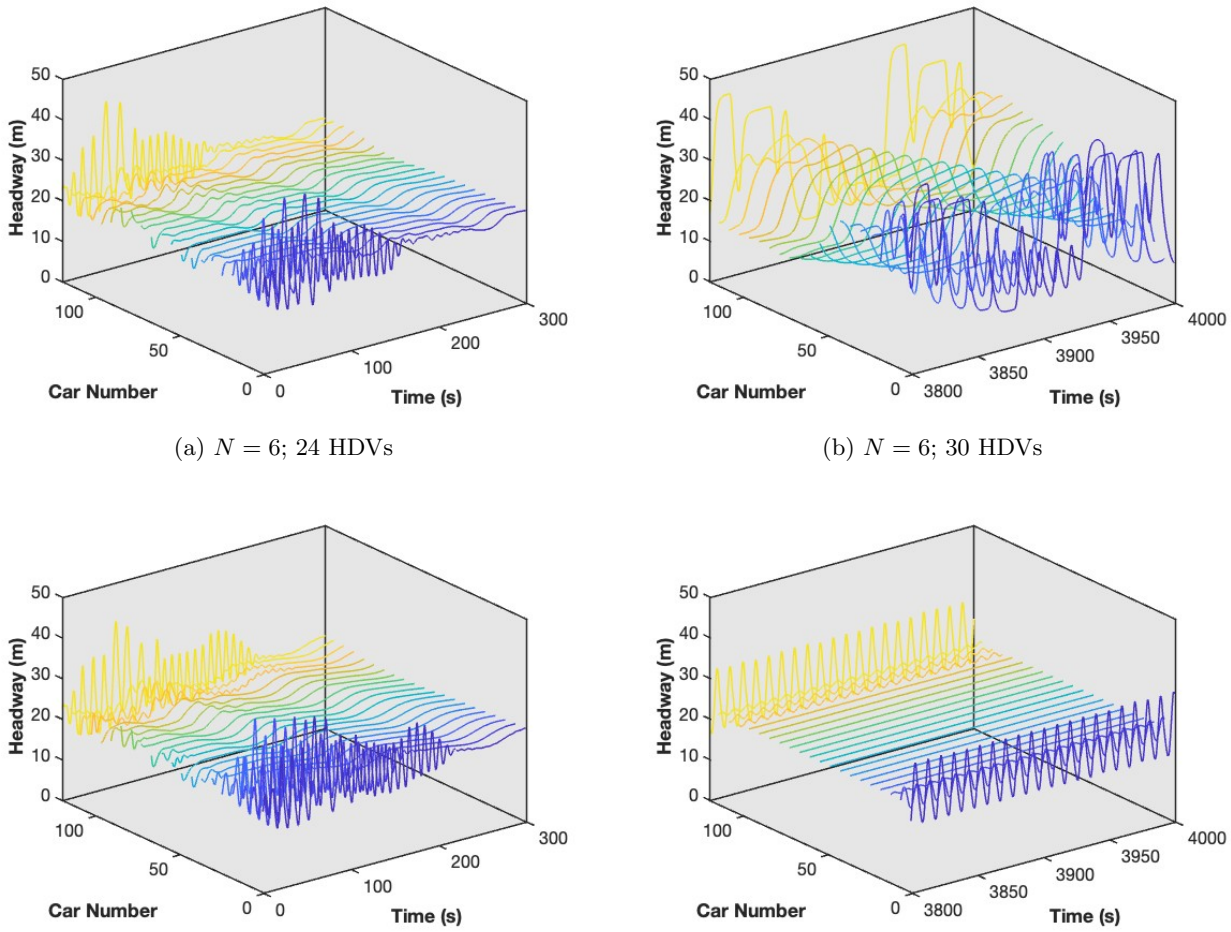

(a) $N = 6$; 24 HDVs

(b) $N = 6$; 30 HDVs

(c) $N = 8$; 32 HDVs

(d) $N = 8$; 40 HDVs

FIGURE 3.13. Headway plots for segregated traffic with CAV platoons of size $N = 6$ with 30 and 36 HDVs and CAV platoons of size $N = 8$ with 32 and 40 HDVs.

speed variation of HDVs is smaller when they are positioned closer to the tail CAV of the platoons, suggesting that HDVs are also prone to string instability.

3.4.3.2. *Evenly mixed CAV platoons and HDVs.* Another appraoch to distributing the vehicles is to mix CAV platoons and HDVs as evenly as possible, i.e. each platoon is follow by a fixed number of HDVs. We again assume that the CAV platoons are not connected, as the distance between platoon leaders is longer than flows of only CAV platoons, which could result in increased delays. Figure 3.14 is the headway plots for evenly mixed traffic, where CAV platoons of size $N = 6$ are followed by 2 or 3 HDVs, and CAV platoons of size $N = 8$ are followed by 5 or 6 HDVs.

REMARK 3.4.3. *One of the platoons may be followed by a different number of HDVs to balance the distribution.*

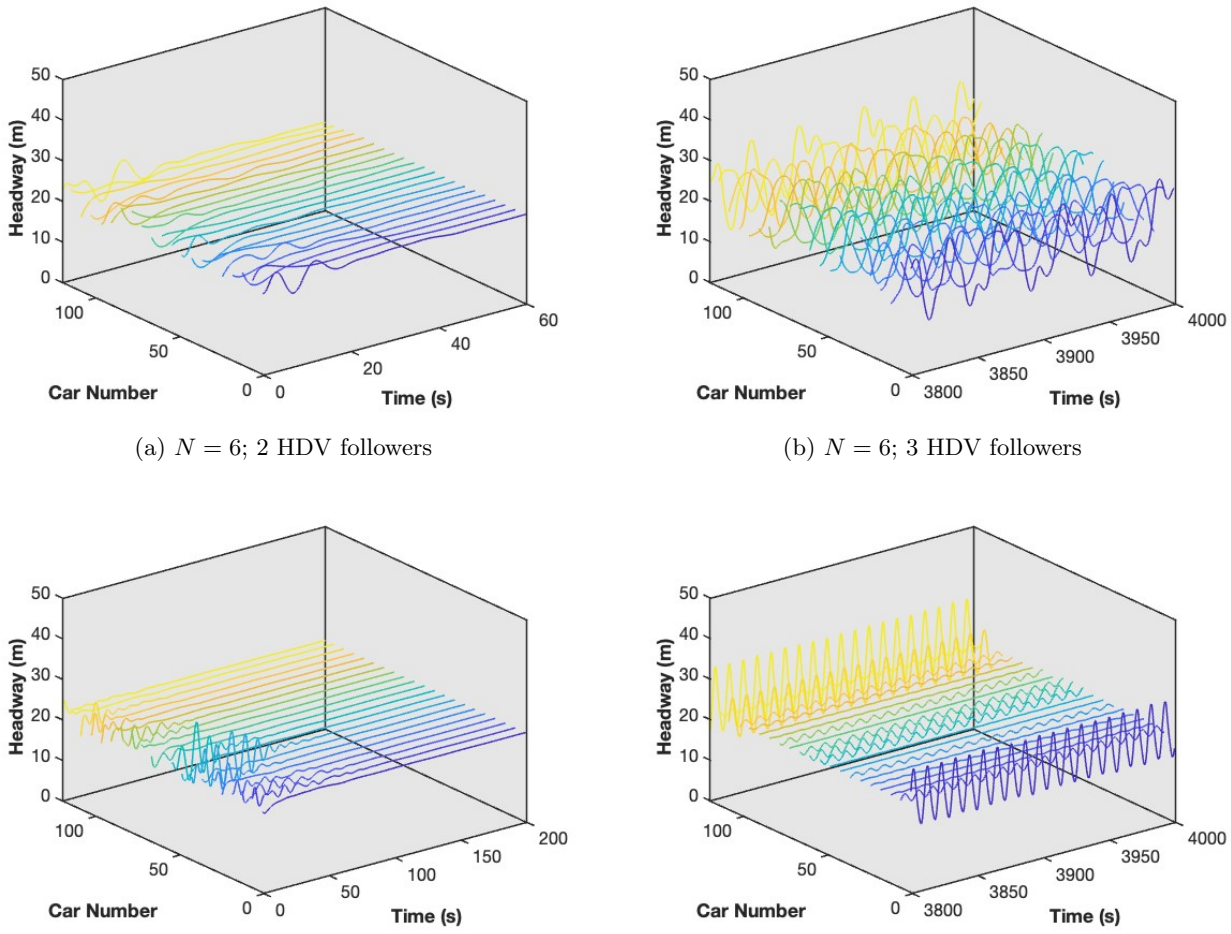

(a) $N = 6$; 2 HDV followers

(b) $N = 6$; 3 HDV followers

(c) $N = 8$; 5 HDV followers

(d) $N = 8$; 6 HDV followers

FIGURE 3.14. Headway plots for evenly mixed traffic with each CAV platoon of size $N = 6$ followed by 2 or 3 HDVs, and CAV platoon of size $N = 8$ followed by 5 or 6 HDVs.

From this simulation, we observed that in evenly mixed distributions, platoons of size $N = 6$ can stabilize up to 30 HDVs, while platoons of size $N = 8$ can stabilize up to 48 HDVs. This suggests that larger platoons act as more effective controllers of traffic stability. However, in scenarios with segregated distributions of $N = 8$ with 40 HDVs, the traffic flow is nearly stable, indicating that the improvements provided by the even distribution are relatively minor. where stability is not fully

achieved, the speed variation among HDVs decreases more significantly when they are positioned closer to the platoons, consistent with previous observations.

3.5. Conclusions

In this chapter, we have extended a recently proposed single platoon CF model to accommodate multiple platoons. By treating the leading vehicle of each platoon considered as control inputs, we developed two distinct control designs that account for varying degrees of connectivity between platoons. We showed that our proposed multi-platoon models are consistent with foundational car-following models when the platoon size is reduced to 1.

Through linear stability analysis, we demonstrated that both platoon size and the level of inter-platoon communication can enhance system stability. The results of numerical experiments with varied platoon size and connectivity are consistent with theoretical analysis. Furthermore, when testing configurations that mixed CAV platoons with HDVs, we observed that HDVs benefit from following CAV platoons—even without specific design considerations for HDV control.

A notable outcome of our analysis is that the influence of inter-platoon connections diminishes as platoon sizes increase. This suggests that, from a manufacturing standpoint, enhancing V2V communication within platoons should be prioritized over V2I communications. Another finding is that the stability of mixed traffic flow exhibits similar characteristics in scenarios where CAV platoons are either evenly distributed or segregated—a result that consists with a study of macroscopic models of mixed flow [20].

This chapter provides a solid foundation for future innovations in CAV technologies and opens several avenues for further exploration. Integration with other control strategies, such as feedback and optimal control, could significantly enhance stability, safety, and comfort for travelers. Additionally, addressing fairness within the model and considering dynamic leader switching and platoon reformation could lead to more practical and equitable applications. Extending the proposed platoon models to accommodate more complex traffic scenarios, such as multi-lane roads and signalized intersections, would broaden the models' applicability.

CHAPTER 4

PDE models: Macroscopic models for CAVs and HDVs

4.1. Introduction and Review of Related Work

4.1.1. Hydrodynamic traffic flow models. Hydrodynamic traffic flow models, often given in the form of partial differential equations (PDEs) have been widely studied in the traffic science literature. They have wide applications and are often used in traffic simulation, state estimation and control design. The most classic of them is the Lighthill-Whitham-Richards (LWR) model [36, 54], which has the form

$$\rho_t + (\rho V(\rho))_x = 0, \tag{4.1}$$

where ρ is the density of traffic at location x and time t, and $V(\rho)$ is the equilibrium velocity as a function of density. The LWR model is essentially a scalar conservation law endowed with a equation of state that captures average driver behavior under stationary (or equilibrium) conditions. The LWR model is capable of modeling transitions from one stationary state to another, in the form of shock or acceleration waves. However, it lacks the ability to model some notable traffic flow phenomena, such as stop-and-go waves and traffic hysteresis. Various models, collectively known as higher-order traffic flow models, have been proposed to overcome LWR model's deficiencies. For example, analogous to shallow channel water flows, Payne and Whitham [50, 68] respectively introduced a momentum equation to capture speed evolution away from equilibrium, and proposed the first higher-order model:

$$\begin{cases} \rho_t + (\rho v)_x = 0, \\ v_t + v v_x = \frac{V(\rho) - v}{\tau} - \frac{c_0^2}{\rho}\rho_x, \end{cases} \tag{4.2}$$

where τ is a relaxation time constant and $c_0 < 0$ is the "traffic sound speed". But this model has two main drawbacks: it can produce negative travel speed ('wrong way travel') and traffic

information can travel faster than vehicles, which violates the anisotropic property of traffic flow—that is, vehicles cannot push other vehicles from behind to speed them up. To solve these problems, there are two models independently introduced in [1,76], and the inhomogeneous Aw-Rascle-Zhang (ARZ) model has the form:

$$\begin{cases} \rho_t + (\rho v)_x = 0, \\ (v + h(\rho))_t + v(v + h(\rho))_x = \frac{V(\rho) - v}{\tau}, \end{cases} \tag{4.3}$$

where the constant c_0 in PW model is substituted by the convective derivative $(\partial_t + v\partial_x)$ of the pressure function $h(\rho)$ accounting for drivers' anticipation of downstream density changes.

The ARZ model has been widely used and studied since it was first proposed. Theoretical and numerical solutions of the ARZ model have been studied in e.g. [28,39,41]. Others have extended the ARZ model: for example, Lebacque et al [29] generalised the ARZ model to the generic second order models (GSOM) where the pressure term is generalised to a non-linear velocity term. The GSOM model have then been used for data fitting [11] and extended with non-local densities [5,17].

4.1.2. Multi-class hydrodynamic traffic flow models. Real-world traffic has vehicles of different types and performances, which can be categorized into vehicle classes. Each class of vehicles may interact with others in different ways and this can be captured by extending the aforementioned models to multi-class hydrodynamic traffic flow models. Starting with an extension of the LWR model, Wong and Wong [69] proposed a multi-class LWR model with heterogeneous drivers characterized by their choice of free-flow speeds. In particular, they gave an isotropic case where the speed of each class is a function of the total density. In a separate work, Zhang and Jin [75] proposed a multi-class LWR model considering critical density such that when traffic concentration reached a critical value, all the class of vehicles are mixed together and move as a group, and below the critical density the model is similar to Wong and Wong's model. Ngoduy and Liu [49] proposed a generalized multi-class first-order simulation model based on an approximate Riemann solver, which is able to explain certain non-linear traffic phenomena on freeways. Logghe and Immers [38] proposed a new model where vehicle classes interact in a non-cooperative way, where slow vehicles act as moving bottlenecks for fast vehicles while fast vehicles have no influence on slow vehicles. Such relations have been previous presented in [44]. Qian et al [52] developed a macroscopic heterogeneous traffic flow model with pragmatic cross-class interaction rules.

There are also studies that proposed non-equilibrium hydrodynamic models for mixed traffic flow, e.g. [19, 42, 45, 46, 48]. Specifically, Ngoduy et al [48] proposed a multi-class gas-kinetic model where one class of vehicles are able to receive a warning massage when there is downstream congestion and further extended it in [45,46] to include cooperative adaptive cruise control (CACC). Mohan and Ramadurai [42] extends the ARZ model to a multi-class model using area occupancy (AO) which can capture the unique phenomena in lane-free traffic. Huang et al [19] proposed a multi-class model where human driven vehicles (HDVs) are modeled by the ARZ model and CAVs are modeled by a mean-field game. They also performed linear stability analysis for the mean-field game model.

4.1.3. CAVs as agents for traffic stabilization. Traffic flow of HDVs can be unstable even without an external disturbance. For example, in [60], a field experiment on a ring road with human driven vehicles showed that stop-and-go waves can arise without the presence of any bottlenecks when there are sufficient number of vehicles on the road. A recent field experiment, on the other hand, showed that such stop-and-go waves can be eliminated with a single AV (Autonomous Vehicle) as a control agent to pace HDV traffic for the vehicles involved [59]. Such improvements were also found in a larger field experiment of over 100 CAVs [30]. This stabilization effect of an AV or CAVs as a control agent has also been widely studied through traffic simulation using microscopic car-following models, e.g. [6, 67, 78]. In these studies, it is shown that a single AV can stabilize multiple HDVs on a single-lane road by using its sensing capabilities and feedback control to adjust its speed.

4.1.4. The main contributions of this chapter. In this chapter, we enhance the understanding on the look-ahead effect of CAVs in traffic flow modelling by extending the ARZ model with a non-local density parameter, which simulates the forward-looking capabilities of CAVs. This modification allows for a more realistic representation of how autonomous technologies might influence traffic flow dynamics.

We undertake a comprehensive theoretical stability analysis using wave perturbation methods and demonstrate that the extended model for CAVs can achieve greater stability over longer look-ahead distances, offering a theoretical foundation for integrating CAVs into traffic systems.

Additionally, we further extend our model to a multi-class framework, accommodating both HDVs and CAVs. This extension is crucial to evaluate the stabilization effect of CAVs in various traffic conditions with presence of HDVs. Through extensive simulations referencing the studies above, we evaluate how different configurations of look-ahead distances and vehicle distributions impact traffic flow stability.

The findings of this study contribute to the ongoing discussions on traffic management in the mixed autonomy environments. One of them suggests that moderate look-ahead distances might provide optimal stability conditions. Another notable finding is that with a relatively low penetration rate of CAVs, the mixed flow can be effectively stabilized, which is consistent with previous studies. Furthermore, evenly distributed CAVs achieve marginally better stabilization results compared to segregated distributions.

The remainder of the chapter is organized as follows: Section 4.2 introduces the modified ARZ model and interprets it as a model for CAVs. Section 4.3 gives a stability analysis of the model using wave perturbation. Section 4.4 formulates a multi-class extension of the modified ARZ model for mixed CAV-HDV traffic and in Section 4.5 parameters of both models are analysed via numerical experiments to test the stability of CAVs under different conditions. Lastly in Section 4.6 conclusion is drawn and directions of future research are proposed.

4.2. An extended ARZ model with look-ahead effect

We first extend the ARZ model to take into account the look-ahead capability of CAVs without explicitly modeling CAVs and HDVs as distinct classes. Here we assume that the CAVs are all equipped with range sensors and vehicle to vehicle communication to enable them to observe the density of a certain distance ahead, say L_D. A visualised demonstration of this is given in **Figure 4.1**.

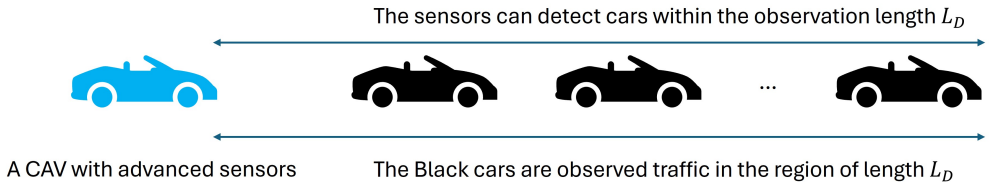

FIGURE 4.1. A CAV's front observation of the traffic density of a certain distance in front.

Instead of responding to the motion of the immediate vehicle in front, a CAV can take advantage of this look-ahead capability and adopt a speed that is based on the average traffic condition within this look-ahead distance, therefore reducing over- or under- reaction and smoothing its trajectory. This will in turn lead to greater stability of traffic. Following this argument, we modify the Aw-Rascle-Zhang model with a new relaxation term that takes into account this look-ahead effect on traffic flow as follows:

$$\begin{cases} \rho_t + (\rho v)_x = 0, \\ (v + h(\rho))_t + v(v + h(\rho))_x = \dfrac{v - V(\rho^*)}{\tau}, \\ \rho^*(L_D) = \dfrac{\int_x^{x+L_D} \rho(t,\xi)d\xi}{L_D}, \end{cases} \tag{4.4}$$

where the relaxation of v is toward an equilibrium speed $V(\rho^*)$ with ρ^* as the average traffic density in the observation region $[x, x + L_D]$. The observed average density is calculated by integration. Moreover, if L_D goes to 0 the model reduces to the original ARZ model. We can also generalize the average density with a weight function for biased observation:

REMARK 4.2.1. *A more general weighted average density $\rho^*(L_D, w)$ with weight function $w(x)$ can be defined as*

$$\rho^*(L_D, w) = \frac{\int_x^{x+L_D} w(\xi)\rho(t,\xi)d\xi}{L_D}, \tag{4.5}$$

where $w(x)$ satisfies $\int_x^{x+L_D} w(\xi)d\xi = 1/L_D$. With the weighted density, CAVs are considering vehicles in front with different sensitivities, similar to the microscopic multi-following model in [31].

With the look-ahead (weighted) average density we are primarily focusing on the CACC logic in CAVs. There are many other complex dynamics and controls which can be implemented into the model (4.4).

Additionally for periodic boundary conditions (i.e. traffic on a ring road), partial observation (look-ahead) is equivalent to full observation (look-ahead of the entire road) when $L_D = L$, the length of the ring road.

For readers who are interested in the theoretical analysis such as solution existence, this model can be implicitly written as the non-local traffic model in [17] that is proven well defined under certain constraints.

4.3. Stability analysis of the extended ARZ model

In this section we will follow the classic wave perturbation analysis approach [26] [12] [53] to analyze the stability of the extended ARZ model (4.4).

For a given initial state (ρ_0, v_0), the steady state solution of the ARZ model is $(\rho, v) = (\rho_0, V(\rho_0))$ for some $0 < \rho_0 < \rho_j$ where ρ_j is the jam density. Now assume that the initial condition is perturbed by a small periodic disturbance:

$$\rho = \rho_0 + \tilde{\rho};\ v = V(\rho_0) + \tilde{v}, \tag{4.6}$$

where

$$\tilde{\rho} = Re^{ikx+\sigma t};\ \tilde{v} = Ve^{ikx+\sigma t} \tag{4.7}$$

with R, V has infinitesimal constant scales, and k, σ are constants for the perturbation's frequency and amplitude, respectively.

By neglecting second or higher order terms of R and V we can derive a linear system

$$\begin{bmatrix} \sigma + ik\psi & ik\rho_0 \\ \sigma\phi + ik\psi\phi - \frac{\zeta}{\tau} & \sigma + ik\psi + \frac{1}{\tau} \end{bmatrix} \begin{bmatrix} R \\ U \end{bmatrix} = \begin{bmatrix} 0 \\ 0 \end{bmatrix} \tag{4.8}$$

where $\psi = V(\rho_0) > 0$, $\phi = h'(\rho) > 0$, $\zeta = (e^{ikL_D} - 1)V'(\rho)/(ikL_D)$.

Follow the calculation process in [53], we can deduce that traffic is stable when

$$h'(\rho) + \frac{|\sin(kL_D)|}{kL_D} V'(\rho) > 0 \tag{4.9}$$

Since $|\sin x|/x$ is a decreasing function of x, this equation implies that with certain level of oscillation frequency, stability criteria does not depend on τ and the range of stability can be increased with L_D.

REMARK 4.3.1. *In particular if $\rho(x + L) = \rho(x)$ for all $x \in \mathbb{R}$, then if $L_D = L$ we have full observation of the road and the model will be always stable. In this case $\rho^* = \rho_0$ which implies that all the vehicles are relaxing toward equilibrium speed.*

4.4. A multiclass extension of the ARZ model with look-ahead effect

In this section, we propose a model for mixed autonomy traffic where HDVs and CAVs are modeled as distinctive classes. Similar to [19], in our model the HDVs are reacting to total density of traffic at its position. If we let ρ^h denote density of HDVs and ρ^c denote the density of CAVs, then the model has the form

$$
\begin{cases}
\rho_t^h + (\rho^h v^h)_x = 0, & \text{(4.10a)}\\
\left(v^h + h(\rho^s)\right)_t + v^h \left(v^h + h(\rho^s)\right)_x = \dfrac{v^h - V(\rho^s)}{\tau}, & \text{(4.10b)}\\
\rho_t^c + (\rho^c v^c)_x = 0, & \text{(4.10c)}\\
\left(v^c + h(\rho^s)\right)_t + v^c \left(v^c + h(\rho^s)\right)_x = \dfrac{v^c - V(\rho^*)}{\tau}, & \text{(4.10d)}\\
\rho^s = \rho^h + \rho^c, & \text{(4.10e)}
\end{cases}
$$

where v^h is the speed of HDVs and v^c is the speed of CAVs. To highlight the look-ahead effect, for the CAVs we assume that they have the same pressure function and relaxation constant as HDVs. With similar reasons we assume that CAVs and HDVs follow the same FD. For such mixed flow the stability can depend on the ratio and distribution of vehicles, and the control method of CAVs, which means that it is hard to obtain the stability condition analytically for the traffic flow model given in (4.10). In this chapter, we resort to numerical solutions of (4.10) to explore the stability properties of this multi-class non-equilibrium model, which will be presented in the next section.

REMARK 4.4.1. *Practically, in mixed autonomy CAVs might be capable to observe both density and speed of surrounding HDVs to change their speed accordingly, which means the pressure term and relaxation term can be defined with consideration of the density of HDVs. We will consider such extensions in future work.*

4.5. Numerical solutions

In order to obtain numerical solutions for (4.4) and (4.10), we adapted a forward scheme with an approximate Riemann solver in [53] that has low computation cost and preserves properties of finite volume methods. To calculate the average density, we use a Riemann sum to give an estimation of the integration term. Given Δt, Δx as time and space step size, $q = \rho(v + h(\rho))$ as a

conserved flux variable, i, n as space step variable and time step variable, and suppose that $L_D/\Delta t$ is a non-negative integer, then the update rule for approximate solutions of (4.4) can be written as

$$\begin{cases} \rho_i^{n+1} = \rho_i^n - \dfrac{\Delta t}{\Delta x}\left((F_\rho)^n_{i+\frac{1}{2}} - (F_\rho)^n_{i-\frac{1}{2}}\right) & \text{(4.11a)} \\ \rho_i^* = \dfrac{\sum_{j=1}^{L_D/\Delta t} \rho_j^{n+1}}{L_D/\Delta t} & \text{(4.11b)} \\ q_i^{n+1} = q_i^n - \dfrac{\Delta t}{\Delta x}\left((F_q)^n_{i+\frac{1}{2}} - (F_q)^n_{i-\frac{1}{2}}\right) - \dfrac{\Delta t}{\tau}\left(V(\rho_i^*) + h(\rho_i^{n+1})\right) & \text{(4.11c)} \end{cases}$$

where the update of the approximated flow q_i^{n+1} is calculated after the update of the approximated density ρ_i^{n+1}, and the update of the relaxation term adopts an implicit scheme to improve numerical stability. The average density ρ_i^* is calculated by Riemann sum and the numerical fluxes $(F_\rho)^n_{i+\frac{1}{2}}, (F_q)^n_{i+\frac{1}{2}}$ are calculated by the Harten, Lax and van Leer (HLL) approximate Riemann solver [18]. The update rule for approximate solutions of (4.10) can be similarly written by separately updating solutions of HDVs and CAVs using (4.11).

For the model parameter values, we assumed that vehicles are on a ring road with length $L = 1000$ meters, and set $\Delta t = 0.05$s, $\Delta x = 5$m, $\tau = 3$s, $h(\rho) = 8 * ((\rho - 10)/(140 - \rho))^{1/2}$m/s, similar to [19]. The equilibrium speed model is a smooth function that combined the Greenshields model [16] and the Triangular FD model [7]:

$$V(\rho) = \begin{cases} v_f, & \text{if } \rho \le \rho_f; \\ v_f\left(1 - \dfrac{\rho - \rho_f}{\rho_j - \rho_f}\right), & \text{if } \rho_f \le \rho \le \rho_j; \\ 0, & \text{if } \rho \ge \rho_j, \end{cases} \tag{4.12}$$

where $\rho_f = 10$veh/km is the free flow density, $\rho_j = 140$veh/km is the jam density and $v_f = 20$m/s is the free flow speed. The initial density is a sinusoidal wave perturbation of equilibrium state similar to [19] as well:

$$\rho_0(x) = 0.4 * \rho_j + 0.1 * \rho_j * \sin(2\pi x/L), \tag{4.13}$$

where for mixed flow we substitute ρ by ρ^s. The initial velocity is then set as $v_0(x) = V(\rho_0(x))$. In the following subsections we will use two cases to evaluate the asymptotic stability of both models under different L_D and vehicle mixes.

4.5.1. Investigation of the look-ahead effect. In this scenario we evaluate the look-ahead distance L_D on the convergence of the extended ARZ model. We will consider $L_D = 15, 100, 1000$m and compare the model results with those from the ARZ model ($L_D \to 0^+$). For $L_D = 0^+, 100$m we set the time duration as $T = 600$s and the others as $T = 1200$s. The numerical results of density and velocity evolution are shown in **Figures 4.2-4.5**.

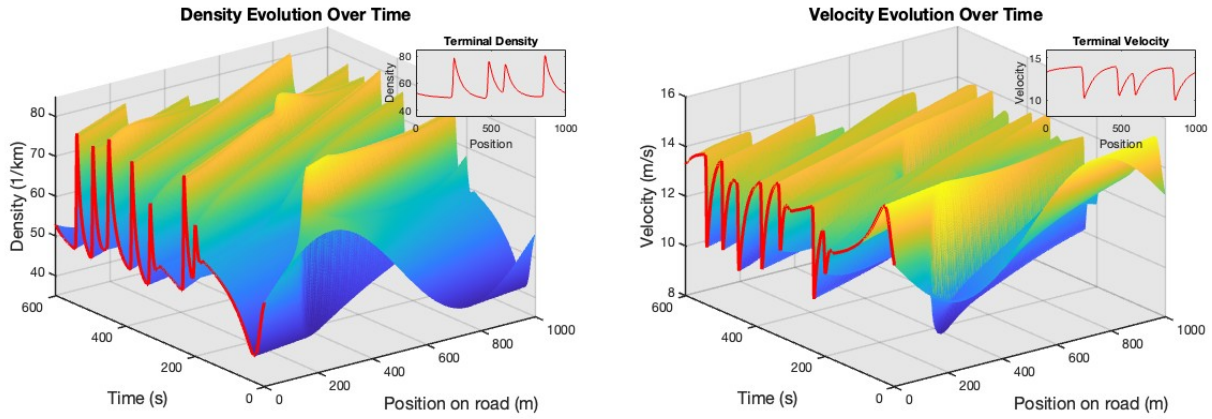

(a) Density evolution

(b) Velocity evolution

FIGURE 4.2. Density and velocity evolution of the ARZ model ($L_D \to 0$), where the flow is not stable.

From the numerical results, we can observe that in all cases look-ahead helps stabilizing traffic, as the only unstable case is when $L_D \to 0^+$. However, longer look-ahead distance is not equivalent to faster convergence to equilibrium state. With full observation, i.e. $L_D = 1000$m, or a shorter partial observation ($L_D = 15$m) the convergence speed is much slower than with $L_D = 100$m. In the case of $L_D = 15$m, the look-ahead effect is not significant since this is no better than follow one-vehicle ahead. With the much longer L_D, the redundant information from far away is also built into drivers' response, and hence can be detrimental rather than beneficial to traffic stability when traffic conditions vary significantly over space. There seems to be a theoretical optimal look-ahead distance for achieving greater convergence and traffic stability, which may depend on parameter

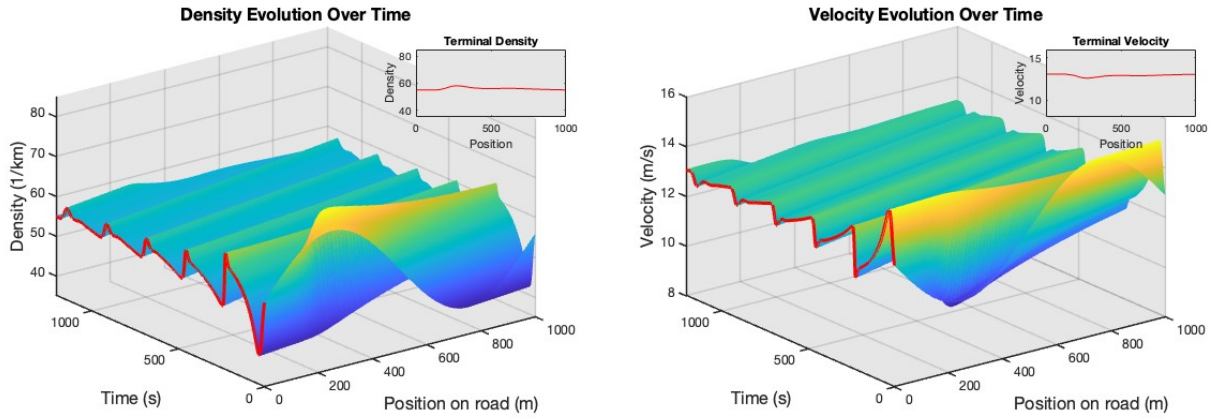

(a) Density evolution (b) Velocity evolution

FIGURE 4.3. Density and velocity evolution of the modified model with $L_D = 15$m.

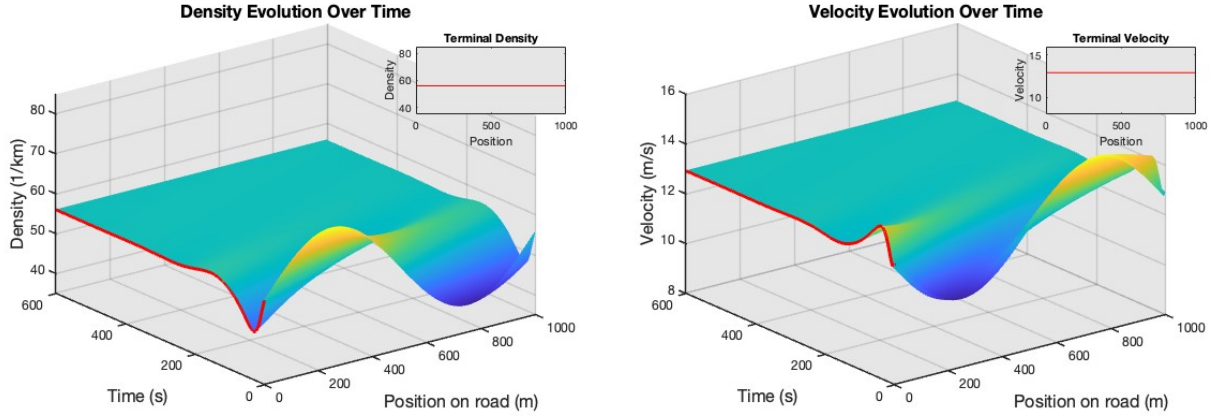

(a) Density evolution (b) Velocity evolution

FIGURE 4.4. Density and velocity evolution of the modified model with $L_D = 100$m.

settings and even initial and boundary traffic conditions. We will explore this problem in our future work.

4.5.2. Investigation of stability in mixed autonomy traffic. In this scenario we investigate the potential of using CAVs to smooth and stabilize mixed traffic flow, considering two different spatial distributions of CAVs in the traffic mix.

4.5.2.1. *Even distribution.* We first consider CAVs evenly distributed in the mixed traffic with penetration rates of 10%, 20%, 40%. Based on the results of the single-class model, we choose the observation distance $L_D = 100$m for CAVs. For 10% and 20% penetration rates we set the time

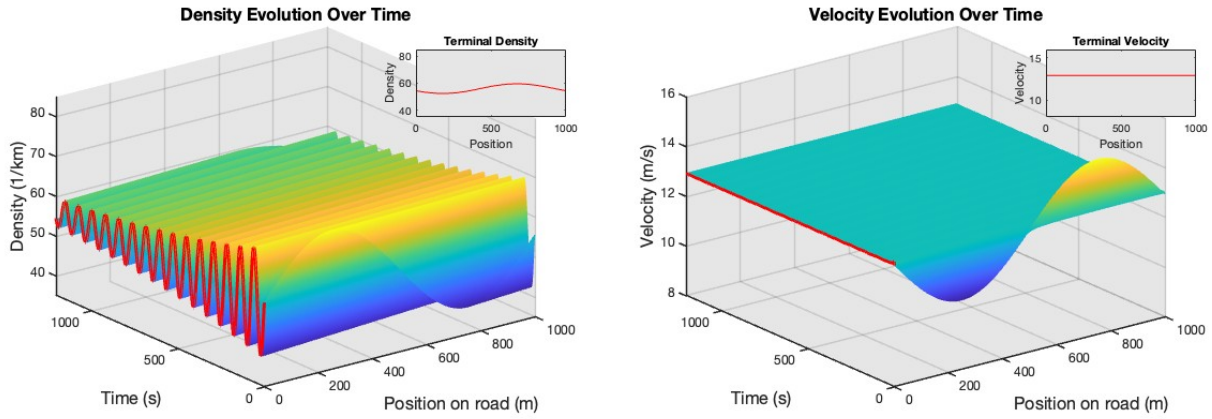

(a) Density evolution

(b) Velocity evolution

FIGURE 4.5. Density and velocity evolution of the modified model with $L_D = 1000$m.

duration to be $T = 1200$s and for 40% we set $T = 600$s. The numerical results of density and velocity evolution are shown in **Figures 4.6-4.8**.

REMARK 4.5.1. *For the mixed plot we plot the evolution of the total density and the HDVs' velocity, since traffic flow of pure CAVs are already shown stable.*

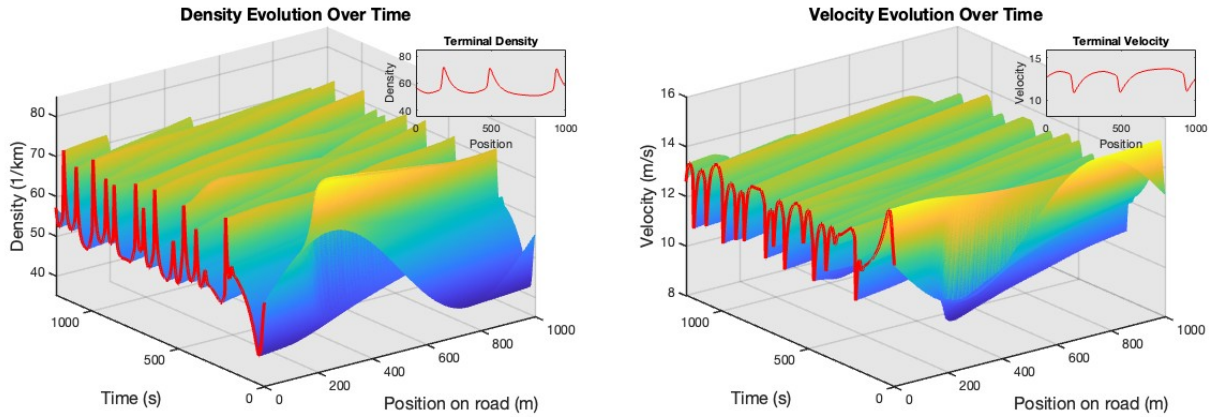

(a) Density evolution

(b) Velocity evolution

FIGURE 4.6. Density and velocity evolution of the mixed flow model with 10% of CAVs evenly distributed.

From these results, we can observe that 20 percent of CAVs can stabilize the mixed flow to smaller oscillations, and 40 percent of CAVs has faster convergence to equilibrium state, while 10

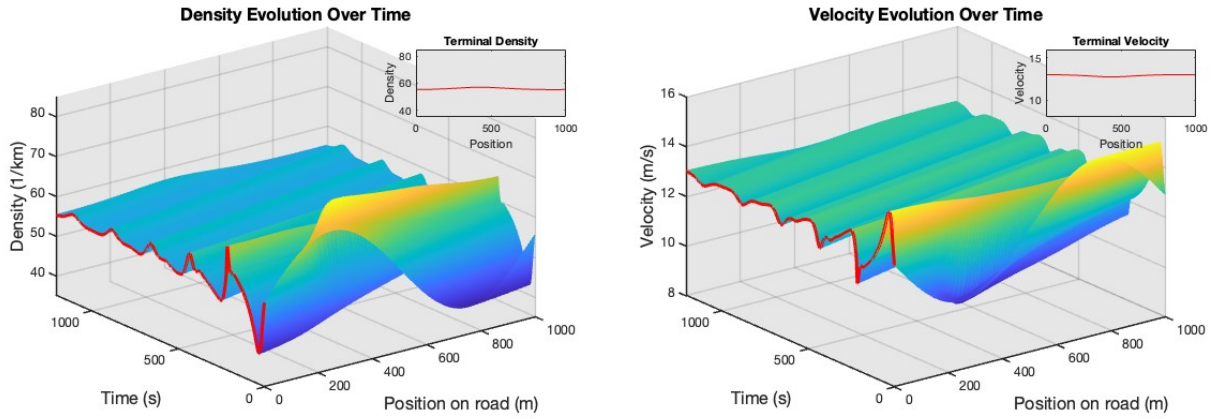

(a) Density evolution

(b) Velocity evolution

FIGURE 4.7. Density and velocity evolution of the mixed flow model with 20% of CAVs evenly distributed.

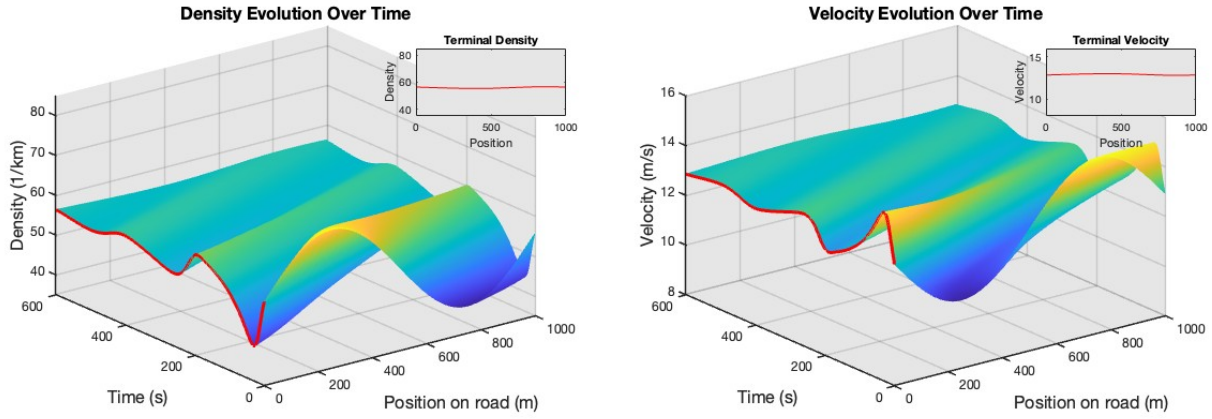

(a) Density evolution

(b) Velocity evolution

FIGURE 4.8. Density and velocity evolution of the mixed flow model with 40% of CAVs evenly distributed.

percent of CAVs fails to stabilize the traffic. Such results are consistent with those from a similar study [19].

4.5.2.2. *Segregated distribution.* Now we consider another type of distribution such that CAVs and HDVs are segregated into two parts. With the same penetration rates, we let CAVs concentrate at around $x = 500$m and HDVs concentrate at the remaining locations. In details, the initial density

of CAVs is given as

$$\rho^c(x) = \begin{cases} 0.999\rho^s, & \text{if } \frac{1-r}{2}L < x < \frac{1+r}{2}L, \\ 0.001\rho^s, & \text{otherwise.} \end{cases} \tag{4.14}$$

where r is the percentage of CAVs, and ρ^h can be calculated by $\rho^h = \rho^s - \rho^c$. The small densities is designed for numerical stability. We set the same simulation time as in the evenly distributed case. The numerical results of density and velocity evolution are shown in **Figures 4.9-4.11**.

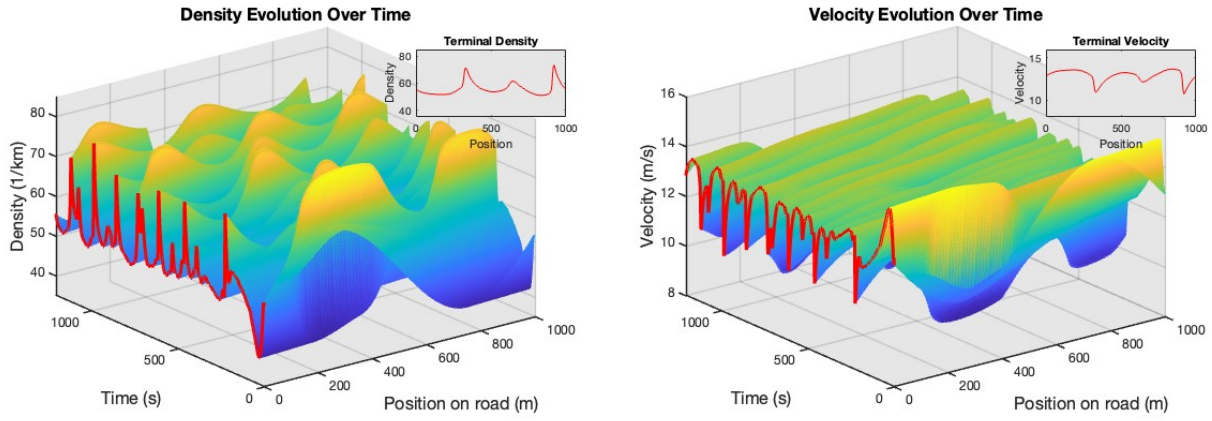

(a) Density evolution

(b) Velocity evolution

FIGURE 4.9. Density and velocity evolution of the mixed flow model with 10% of concentrated CAVs.

These results showed that the segregated distributions of mixed flow have similar asymptotic behaviors as even distributions. The main difference is that the initial waves have larger scales for segregated distributions where the HDVs are concentrated, since HDV traffic is less stable than CAV traffic. Overall the convergence of mixed traffic is slower than the results obtained in [19], possibly due to large oscillations and inadequate information utilized from HDVs. One possible improvement is to add predictive or feedback controls as previously investigated in car-following models e.g. [25, 82].

4.6. Concluding remarks

This chapter make extensions to a second order non-equilibrium traffic flow model, i.e. the ARZ model, to take into account the look-ahead capabilities of CAVs, either in a single-class or multi-class

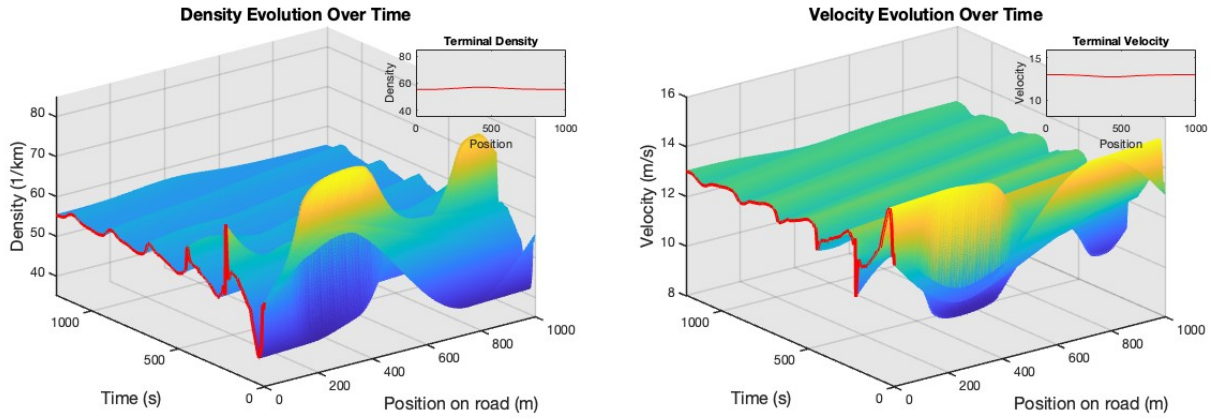

(a) Density evolution

(b) Velocity evolution

FIGURE 4.10. Density and velocity evolution of the mixed flow model with 20% of concentrated CAVs.

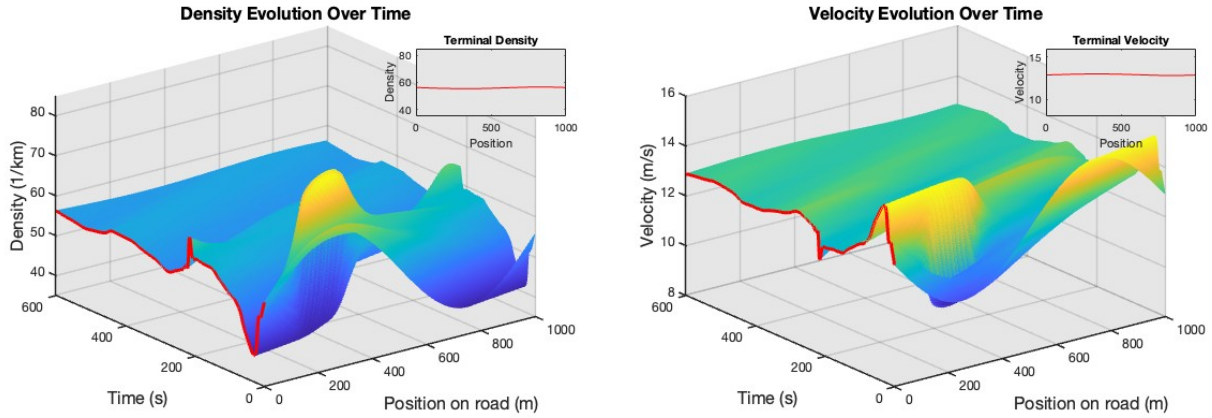

(a) Density evolution

(b) Velocity evolution

FIGURE 4.11. Density and velocity evolution of the mixed flow model with 40% of concentrated CAVs.

context. The look-ahead effect is captured by a modification of the relaxation term, which can be interpreted as CAVs attempt to adopt a target speed based on the average traffic conditions within its spatial observation range, similar to multi-following microscopic traffic models. The stability properties of both extended models are analysed through wave perturbation analysis, and the results show that a longer observation range yields a less restrictive stability condition. Numerical solution using forward schemes with approximate Riemann solvers is provided,and numerical experiments are carried out to examine the effects of various parameters and the spatial distribution of CAVS

on both the stability of mixed autonomy traffic, and CAVs' ability to stabilize mixed traffic flow. It is found that higher penetration rate of CAVs stabilize mixed traffic flow faster, which is consistent with similar studies in [19].

Our study reveals several new insights on mixed autonomy traffic. One interesting finding is that having more information of traffic conditions does not necessarily translate into better control of traffic. In our particular setting, a moderate look-ahead distance of 100m enables faster convergence to equilibrium than having the full observation of road conditions on the entire ring road. Another interesting finding is that the distribution of vehicles have little effect on long-term stability of mixed traffic flow, but the initial oscillations for segregated distribution have larger amplitudes than that in the even distribution case. These insights can help CAV manufacturers design more effective control algorithm that can benefit both parties in mixed autonomy traffic, and traffic engineers to better manage mixed autonomy flow through leveraging the sensing and control capabilities of CAVs.

CHAPTER 5

Conclusions and future work

This dissertation presented a comprehensive investigation into the behavior and stability of CAVs in both homogeneous (fully autonomous) and mixed traffic scenarios involving HDVs. Using a combination of ODE-based CF models and PDE-based macroscopic models, we analyzed different factors' effects on traffic stability, including platoon sizes, communication levels, and look-ahead distances.

The first study introduces a single-platoon car-following model, where vehicles communicate solely with the platoon leader. This model is analyzed through linear stability theory and numerical simulations, showing that improved communication can enhance traffic stability. The second study extends this model to a multi-platoon framework, accommodating various platoon sizes and communication levels between platoons. Theoretical results demonstrate that larger platoons and higher communication capabilities contribute to increased stability, and simulations show that in mixed traffic human-driven vehicles (HDVs) benefit from following CAV platoons. The third study shifts to a macroscopic perspective, extending the ARZ model to capture the dynamics of mixed traffic with CAVs and HDVs. The findings highlight the positive impact of CAVs' look-ahead capabilities on traffic flow stability.

There are several promising directions for future research. One potential avenue is the integration of advanced control strategies, such as MPC and RL, which could further improve the adaptability and performance of CAVs in dynamic traffic environments. Another important area for exploration is the application of these models to multi-lane roads and urban settings, where lane-changing behavior and signalized intersections can occur. Furthermore, conducting field experiments to validate the theoretical and numerical findings of this dissertation would offer valuable insights and refine the models based on empirical data.

To summarize, this dissertation has made considerable contributions to the understanding of CAVs in both homogeneous and mixed traffic systems. The theoretical analyses and simulations

offer a strong foundation for future work in control design and management of CAVs, with the potential to enhance traffic stability and efficiency as CAV technologies continue to develop.

APPENDIX A

Appendices

A.1. Proof of Theorem 2.3.1

In this section we give the proof of Theorem 2.3.1:

PROOF. Similar to proof of 2.3.2, we consider small deviation y_i from the equilibrium solution and neglect higher order. Then we have

$$\ddot{y}_i(t) = a\left[V'(h)(y_{i+1}(t) - y_i(t)) - \dot{y}_i(t)\right],\ y_{N+1} = y_1, \tag{A.1}$$

which is a linear ODE system with N equations. Suppose that λ is an eigenvalue of the system, and ξ_i is the coefficient of y_i with the term $e^{\lambda t}$, then simplified from A.1, λ satisfies

$$\lambda^2 + a\lambda - aV'(h)(\frac{\xi_{i+1}}{\xi_i} - 1) = 0 \tag{A.2}$$

This means $\xi_{i+1}/\xi_i = r$ is fixed for given λ, and note that $\prod_{i=1}^{N}(\xi_{i+1}/\xi_i) = 1$, we have

$$r = e^{\frac{2\pi k}{N}i},\ k = 1, 2, \ldots, N. \tag{A.3}$$

Therefore λ satisfies

$$\lambda^2 + a\lambda - aV'(h)(e^{\frac{2\pi k}{N}i} - 1) = 0, \tag{A.4}$$

for some $k = 1, 2, \ldots, N$. Then, to have a stable system of y_n, the real parts of any λ should be negative. By considering the solution of λ with smaller real parts we have

$$a - \sqrt{\frac{d + \sqrt{d^2 + e^2}}{2}} > 0, \tag{A.5}$$

where $d = a^2 + 4aV'(h)\cos\frac{2\pi k}{N} - 4aV'(h)$ and $e = -4aV'(h)\sin\frac{2\pi k}{N}$. For the system to be stable, we need this condition to be satisfied for every k. Let $\theta \triangleq \frac{2\pi k}{N}$, then (A.5) can be simplified to

$$-V'(h)\cos^2\theta + a\cos\theta + V'(h) - a < 0. \tag{A.6}$$

(A.6) holds if (2.6) holds, otherwise for N sufficiently large we can let $\cos\theta = a/2V'(h)$ and (A.6) will fail. □

A.2. Proof of Theorem 2.3.3

In this section we give the proof of Theorem 2.3.3:

PROOF. Again we consider small deviation y_i from the equilibrium solution and neglect higher order. Then we have

$$\ddot{y}_i(t) = \begin{cases} a\left[V'(h)(y_{i+1}(t) - y_i(t)) - \dot{y}_i(t)\right] + b\left[V'(h)\frac{y_N(t)-y_i(t)}{N-i} - \dot{y}_i(t)\right], \text{ if } i \neq N; \\ (a+b)\left[V'(h)(y_{i+1}(t) - y_i(t)) - \dot{y}_i(t)\right], \text{ if } i = N, \end{cases} \tag{A.7}$$

which is a linear ODE system with N equations. Suppose that λ is an eigenvalue of the system, and ξ_i is the coefficient of y_i with the term $e^{\lambda t}$, then simplified from (A.7), λ satisfies

$$\lambda^2 + (a+b)\lambda - aV'(h)(\frac{\xi_{i+1}}{\xi_i} - 1) - \frac{bV'(h)}{N-i}(\frac{\xi_N}{\xi_i} - 1) = 0, \text{ if } i \neq N \tag{A.8}$$

and

$$\lambda^2 + (a+b)\lambda - (a+b)V'(h)(\frac{\xi_1}{\xi_N} - 1) = 0. \tag{A.9}$$

When N is very large ($N \to \infty$), $bV'(h)/(N-i)$ is very small for most i, and the last term of (A.8) has minimal effect. This means ξ_{i+1}/ξ_i will converge to eigenvalues given in (A.3). Then λ will converge to values given by

$$\lambda^2 + (a+b)\lambda - aV'(h)(e^{\frac{2\pi k}{N}i} - 1) = 0. \tag{A.10}$$

Follow the same steps of previous proof we can find the stability criterion (2.15). □

Bibliography

[1] A. Aw and M. Rascle, *Resurrection of" second order" models of traffic flow*, SIAM journal on applied mathematics, 60 (2000), pp. 916–938.

[2] M. Bando, K. Hasebe, K. Nakanishi, A. Nakayama, A. Shibata, and Y. Sugiyama, *Phenomenological study of dynamical model of traffic flow*, Journal de Physique I, 5 (1995), pp. 1389–1399.

[3] M. Bando, K. Hasebe, A. Nakayama, A. Shibata, and Y. Sugiyama, *Dynamical model of traffic congestion and numerical simulation*, Physical review E, 51 (1995), p. 1035.

[4] B. Besselink and K. H. Johansson, *String stability and a delay-based spacing policy for vehicle platoons subject to disturbances*, IEEE Transactions on Automatic Control, 62 (2017), pp. 4376–4391.

[5] F. A. Chiarello, J. Friedrich, P. Goatin, and S. Gottlich, *Micro-macro limit of a nonlocal generalized aw-rascle type model*, SIAM Journal on Applied Mathematics, 80 (2020), pp. 1841–1861.

[6] S. Cui, B. Seibold, R. Stern, and D. B. Work, *Stabilizing traffic flow via a single autonomous vehicle: Possibilities and limitations*, in 2017 IEEE Intelligent Vehicles Symposium (IV), IEEE, 2017, pp. 1336–1341.

[7] C. F. Daganzo and N. Geroliminis, *An analytical approximation for the macroscopic fundamental diagram of urban traffic*, Transportation Research Part B: Methodological, 42 (2008), pp. 771–781.

[8] F. de Souza, O. Verbas, and J. Auld, *Mesoscopic traffic flow model for agent-based simulation*, Procedia Computer Science, 151 (2019), pp. 858–863.

[9] M. L. Delle Monache and P. Goatin, *Scalar conservation laws with moving constraints arising in traffic flow modeling: an existence result*, Journal of Differential equations, 257 (2014), pp. 4015–4029.

[10] O. Derbel, T. Peter, H. Zebiri, B. Mourllion, and M. Basset, *Modified intelligent driver model for driver safety and traffic stability improvement*, IFAC Proceedings Volumes, 46 (2013), pp. 744–749.

[11] S. Fan, M. Herty, and B. Seibold, *Comparative model accuracy of a data-fitted generalized aw-rascle-zhang model*, arXiv preprint arXiv:1310.8219, (2013).

[12] M. R. Flynn, A. R. Kasimov, J.-C. Nave, R. R. Rosales, and B. Seibold, *Self-sustained nonlinear waves in traffic flow*, Physical Review E—Statistical, Nonlinear, and Soft Matter Physics, 79 (2009), p. 056113.

[13] F. Gao, S. E. Li, Y. Zheng, and D. Kum, *Robust control of heterogeneous vehicular platoon with uncertain dynamics and communication delay*, IET Intelligent Transport Systems, 10 (2016), pp. 503–513.

[14] S. Gong, J. Shen, and L. Du, *Constrained optimization and distributed computation based car following control of a connected and autonomous vehicle platoon*, Transportation Research Part B: Methodological, 94 (2016), pp. 314–334.

[15] S. Graffione, C. Bersani, R. Sacile, and E. Zero, *Model predictive control of a vehicle platoon*, in 2020 IEEE 15th International Conference of System of Systems Engineering (SoSE), IEEE, 2020, pp. 513–518.

[16] B. D. Greenshields, J. R. Bibbins, W. Channing, and H. H. Miller, *A study of traffic capacity*, in Highway research board proceedings, vol. 14, Washington, DC, 1935, pp. 448–477.

[17] T. Hamori and C. Tan, *On the aw-rascle-zhang traffic models with nonlocal look-ahead interactions*, arXiv preprint arXiv:2403.08643, (2024).

[18] A. Harten, *High resolution schemes for hyperbolic conservation laws*, Journal of computational physics, 135 (1997), pp. 260–278.

[19] K. Huang, X. Di, Q. Du, and X. Chen, *Scalable traffic stability analysis in mixed-autonomy using continuum models*, Transportation research part C: emerging technologies, 111 (2020), pp. 616–630.

[20] S. Hui and M. Zhang, *An anisotropic traffic flow model with look-ahead effect for mixed autonomy traffic*, arXiv preprint arXiv:2407.20554, (2024).

[21] ——, *A new platooning model for connected and autonomous vehicles to improve string stability*, arXiv preprint arXiv:2405.18791, (2024).

[22] S. E. Jabari and H. X. Liu, *A stochastic model of traffic flow: Theoretical foundations*, Transportation Research Part B: Methodological, 46 (2012), pp. 156–174.

[23] D. Jia and D. Ngoduy, *Platoon based cooperative driving model with consideration of realistic inter-vehicle communication*, Transportation Research Part C: Emerging Technologies, 68 (2016), pp. 245–264.

[24] R. Jiang, Q. Wu, and Z. Zhu, *Full velocity difference model for a car-following theory*, Physical Review E, 64 (2001), p. 017101.

[25] Y. Jin and J. Meng, *Dynamical analysis of an optimal velocity model with time-delayed feedback control*, Communications in Nonlinear Science and Numerical Simulation, 90 (2020), p. 105333.

[26] B. S. Kerner and P. Konhauser, *Cluster effect in initially homogeneous traffic flow*, Physical review E, 48 (1993), p. R2335.

[27] H. Lazar, K. Rhoulami, and D. Rahmani, *A review analysis of optimal velocity models*, Periodica Polytechnica Transportation Engineering, 44 (2016), pp. 123–131.

[28] J.-P. Lebacque, S. Mammar, and H. Haj-Salem, *The aw–rascle and zhang's model: Vacuum problems, existence and regularity of the solutions of the riemann problem*, Transportation Research Part B: Methodological, 41 (2007), pp. 710–721.

[29] J.-P. Lebacque, S. Mammar, and H. Haj-Salem, *Generic second order traffic flow modelling*, Transportation and traffic theory, 2007 (2007), pp. 755–776.

[30] J. W. Lee, H. Wang, K. Jang, A. Hayat, M. Bunting, A. Alanqary, W. Barbour, Z. Fu, X. Gong, G. Gunter, et al., *Traffic control via connected and automated vehicles: An open-road field experiment with 100 cavs*, arXiv preprint arXiv:2402.17043, (2024).

[31] H. Lenz, C. Wagner, and R. Sollacher, *Multi-anticipative car-following model*, The European Physical Journal B-Condensed Matter and Complex Systems, 7 (1999), pp. 331–335.

[32] R. J. LeVeque and R. J. Leveque, *Numerical methods for conservation laws*, vol. 214, Springer, 1992.

[33] B. Li, *Stochastic modeling for vehicle platoons (i): Dynamic grouping behavior and online platoon recognition*, Transportation Research Part B: Methodological, 95 (2017), pp. 364–377.

[34] ———, *Stochastic modeling for vehicle platoons (ii): Statistical characteristics*, Transportation Research Part B: Methodological, 95 (2017), pp. 378–393.

[35] Y. Li, Q. Lv, H. Zhu, H. Li, H. Li, S. Hu, S. Yu, and Y. Wang, *Variable time headway policy based platoon control for heterogeneous connected vehicles with external disturbances*, IEEE Transactions on Intelligent Transportation Systems, 23 (2022), pp. 21190–21200.

[36] M. J. Lighthill and G. B. Whitham, *On kinematic waves ii. a theory of traffic flow on long crowded roads*, Proceedings of the Royal Society of London. Series A. Mathematical and Physical Sciences, 229 (1955), pp. 317–345.

[37] T. Liu, L. Lei, K. Zheng, and K. Zhang, *Autonomous platoon control with integrated deep reinforcement learning and dynamic programming*, IEEE Internet of Things Journal, 10 (2022), pp. 5476–5489.

[38] S. Logghe, *Multi-class kinematic wave theory of traffic flow*, Transportation Research Part B: Methodological, 42 (2008), pp. 523–541.

[39] S. Mammar, J.-P. Lebacque, and H. H. Salem, *Riemann problem resolution and godunov scheme for the aw-rascle-zhang model*, Transportation science, 43 (2009), pp. 531–545.

[40] V. Milanés, S. E. Shladover, J. Spring, C. Nowakowski, H. Kawazoe, and M. Nakamura, *Cooperative adaptive cruise control in real traffic situations*, IEEE Transactions on intelligent transportation systems, 15 (2013), pp. 296–305.

[41] S. Mohammadian and F. van Wageningen-Kessels, *Improved numerical method for aw-rascle type continuum traffic flow models*, Transportation Research Record, 2672 (2018), pp. 262–276.

[42] R. Mohan and G. Ramadurai, *Heterogeneous traffic flow modelling using second-order macroscopic continuum model*, Physics Letters A, 381 (2017), pp. 115–123.

[43] A. Nakayama, Y. Sugiyama, and K. Hasebe, *Effect of looking at the car that follows in an optimal velocity model of traffic flow*, Physical Review E, 65 (2001), p. 016112.

[44] G. F. Newell, *A moving bottleneck*, Transportation Research Part B: Methodological, 32 (1998), pp. 531–537.

[45] D. Ngoduy, *Analytical studies on the instabilities of heterogeneous intelligent traffic flow*, Communications in Nonlinear Science and Numerical Simulation, 18 (2013), pp. 2699–2706.

[46] ———, *Instability of cooperative adaptive cruise control traffic flow: A macroscopic approach*, Communications in Nonlinear Science and Numerical Simulation, 18 (2013), pp. 2838–2851.

[47] ———, *Linear stability of a generalized multi-anticipative car following model with time delays*, Communications in Nonlinear Science and Numerical Simulation, 22 (2015), pp. 420–426.

[48] D. Ngoduy, S. Hoogendoorn, and R. Liu, *Continuum modeling of cooperative traffic flow dynamics*, Physica A: Statistical Mechanics and its Applications, 388 (2009), pp. 2705–2716.

[49] D. Ngoduy and R. Liu, *Multiclass first-order simulation model to explain non-linear traffic phenomena*, Physica A: Statistical Mechanics and its Applications, 385 (2007), pp. 667–682.

[50] H. J. Payne, *Model of freeway traffic and control*, Mathematical Model of Public System, (1971), pp. 51–61.

[51] L. A. Pipes, *An operational analysis of traffic dynamics*, Journal of applied physics, 24 (1953), pp. 274–281.

[52] Z. S. Qian, J. Li, X. Li, M. Zhang, and H. Wang, *Modeling heterogeneous traffic flow: A pragmatic approach*, Transportation Research Part B: Methodological, 99 (2017), pp. 183–204.

[53] R. Ramadan, R. R. Rosales, and B. Seibold, *Structural properties of the stability of jamitons*, in Mathematical descriptions of traffic flow: Micro, macro and kinetic models, Springer, 2021, pp. 35–62.

[54] P. I. Richards, *Shock waves on the highway*, Operations research, 4 (1956), pp. 42–51.

[55] Ş. Sabău, C. Oară, S. Warnick, and A. Jadbabaie, *Optimal distributed control for platooning via sparse coprime factorizations*, IEEE Transactions on Automatic Control, 62 (2016), pp. 305–320.

[56] M. Sala and F. Soriguera, *Macroscopic modeling of connected autonomous vehicle platoons under mixed traffic conditions*, Transportation Research Procedia, 47 (2020), pp. 163–170.

[57] B. Seibold, *A mathematical introduction to traffic flow theory*, IPAM Tutorials, (2015).

[58] S. Sheikholeslam and C. A. Desoer, *Longitudinal control of a platoon of vehicles*, in 1990 American control conference, IEEE, 1990, pp. 291–296.

[59] R. E. Stern, S. Cui, M. L. Delle Monache, R. Bhadani, M. Bunting, M. Churchill, N. Hamilton, H. Pohlmann, F. Wu, B. Piccoli, et al., *Dissipation of stop-and-go waves via control of autonomous vehicles: Field experiments*, Transportation Research Part C: Emerging Technologies, 89 (2018), pp. 205–221.

[60] Y. Sugiyama, M. Fukui, M. Kikuchi, K. Hasebe, A. Nakayama, K. Nishinari, S.-i. Tadaki, and S. Yukawa, *Traffic jams without bottlenecks—experimental evidence for the physical mechanism of the formation of a jam*, New journal of physics, 10 (2008), p. 033001.

[61] J. Sun, Z. Zheng, and J. Sun, *The relationship between car following string instability and traffic oscillations in finite-sized platoons and its use in easing congestion via connected and automated vehicles with idm based controller*, Transportation Research Part B: Methodological, 142 (2020), pp. 58–83.

[62] M. Treiber, A. Hennecke, and D. Helbing, *Congested traffic states in empirical observations and microscopic simulations*, Physical review E, 62 (2000), p. 1805.

[63] M. Treiber, A. Kesting, and D. Helbing, *Delays, inaccuracies and anticipation in microscopic traffic models*, Physica A: Statistical Mechanics and its Applications, 360 (2006), pp. 71–88.

[64] S. Tsugawa, S. Kato, and K. Aoki, *An automated truck platoon for energy saving*, in 2011 IEEE/RSJ international conference on intelligent robots and systems, IEEE, 2011, pp. 4109–4114.

[65] A. Vahidi and A. Eskandarian, *Research advances in intelligent collision avoidance and adaptive cruise control*, IEEE transactions on intelligent transportation systems, 4 (2003), pp. 143–153.

[66] E. Walraven, M. T. Spaan, and B. Bakker, *Traffic flow optimization: A reinforcement learning approach*, Engineering Applications of Artificial Intelligence, 52 (2016), pp. 203–212.

[67] J. Wang, Y. Zheng, C. Chen, Q. Xu, and K. Li, *Leading cruise control in mixed traffic flow: System modeling, controllability, and string stability*, IEEE Transactions on Intelligent Transportation Systems, 23 (2021), pp. 12861–12876.

[68] G. B. Whitham, *Linear and nonlinear waves*, vol. 42, John Wiley & Sons, 2011.

[69] G. Wong and S. Wong, *A multi-class traffic flow model–an extension of lwr model with heterogeneous drivers*, Transportation Research Part A: Policy and Practice, 36 (2002), pp. 827–841.

[70] H. Yu and M. Krstic, *Varying speed limit control of aw-rascle-zhang traffic model*, in 2018 21st international conference on intelligent transportation systems (ITSC), IEEE, 2018, pp. 1846–1851.

[71] ———, *Traffic congestion control for aw–rascle–zhang model*, Automatica, 100 (2019), pp. 38–51.

[72] S. Yu, Q. Liu, and X. Li, *Full velocity difference and acceleration model for a car-following theory*, Communications in Nonlinear Science and Numerical Simulation, 18 (2013), pp. 1229–1234.

[73] W. Yu, X. Hua, D. Ngoduy, and W. Wang, *On the assessment of the dynamic platoon and information flow topology on mixed traffic flow under connected environment*, Transportation research part C: emerging technologies, 154 (2023), p. 104265.

[74] W. Yu, D. Ngoduy, X. Hua, and W. Wang, *On the stability of a heterogeneous platoon-based traffic system with multiple anticipations in the presence of connected and automated vehicles*, Transportation Research Part C: Emerging Technologies, 157 (2023), p. 104389.

[75] H. Zhang and W. Jin, *Kinematic wave traffic flow model for mixed traffic*, Transportation Research Record, 1802 (2002), pp. 197–204.

[76] H. M. Zhang, *A non-equilibrium traffic model devoid of gas-like behavior*, Transportation Research Part B: Methodological, 36 (2002), pp. 275–290.

[77] L. Zhang, M. Zhang, J. Wang, X. Li, and W. Zhu, *Internet connected vehicle platoon system modeling and linear stability analysis*, Computer Communications, 174 (2021), pp. 92–100.

[78] C. Zhao, H. Yu, and T. G. Molnar, *Safety-critical traffic control by connected automated vehicles*, Transportation research part C: emerging technologies, 154 (2023), p. 104230.

[79] Y. Zheng, S. E. Li, J. Wang, D. Cao, and K. Li, *Stability and scalability of homogeneous vehicular platoon: Study on the influence of information flow topologies*, IEEE Transactions on intelligent transportation systems, 17 (2015), pp. 14–26.

[80] J. Zhou, Z.-K. Shi, and J.-L. Cao, *Nonlinear analysis of the optimal velocity difference model with reaction-time delay*, Physica A: Statistical Mechanics and its Applications, 396 (2014), pp. 77–87.

[81] S. Zhou, J. Tian, Y.-E. Ge, S. Yu, and R. Jiang, *Experimental features of emissions and fuel consumption in a car-following platoon*, Transportation Research Part D: Transport and Environment, 121 (2023), p. 103823.

[82] Y. Zhou, M. Wang, and S. Ahn, *Distributed model predictive control approach for cooperative car-following with guaranteed local and string stability*, Transportation research part B: methodological, 128 (2019), pp. 69–86.

[83] Z. Zhou, L. Li, X. Qu, and B. Ran, *An autonomous platoon formation strategy to optimize cav car-following stability under periodic disturbance*, Physica A: Statistical Mechanics and its Applications, 626 (2023), p. 129096.

[84] ——, *A self-adaptive idm car-following strategy considering asymptotic stability and damping characteristics*, Physica A: Statistical Mechanics and its Applications, 637 (2024), p. 129539.

[85] W.-X. Zhu and H. M. Zhang, *Analysis of mixed traffic flow with human-driving and autonomous cars based on car-following model*, Physica A: Statistical Mechanics and its Applications, 496 (2018), pp. 274–285.